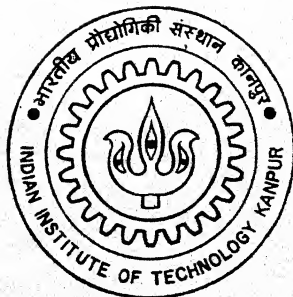


FLOW ABOUT THE BLUFF BODIES BY THE FULL-VORTEX CLOUD APPROACH

by

MANISH KUMAR JAIN



DEPARTMENT OF AEROSPACE ENGINEERING

INDIAN INSTITUTE OF TECHNOLOGY KANPUR

APRIL, 1996

AE

1996

M

JAI

FLO

Flow about the bluff bodies by the full-vortex cloud approach

*A Thesis Submitted
in Partial Fulfillment of the Requirements
for the Degree of
Master of Technology*

*by
Manish Kumar Jain*

to the
DEPARTMENT OF AEROSPACE ENGINEERING
INDIAN INSTITUTE OF TECHNOLOGY, KANPUR

April, 1996

JUL 1996

CENTRAL LIBRARY

~~121749~~
No. A.

AE-1996-M-JAH-FLO



A121749

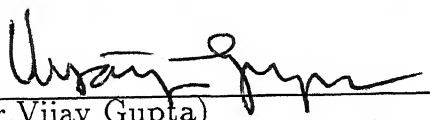
© Copyright 1996

by

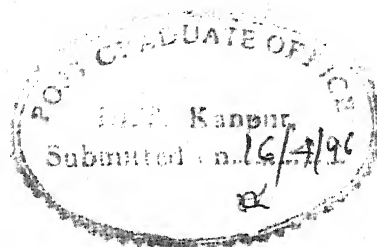
Manish Kumar Jain

CERTIFICATE

Certified that the work contained in the thesis entitled
"Flow about the bluff bodies by the full-vortex cloud approach",
by *"Manish Kumar Jain"*, has been carried out under my
supervision and that this work has not been submitted elsewhere
for a degree.


(Dr. Vijay Gupta)

Department of Aerospace Engineer-
ing,
Indian Institute of Technology,
Kanpur.



April, 1996

Abstract

In the present work, first, a procedure has been developed for the simulation of viscous diffusion in a boundary-layer flow. An operator splitting algorithm has been developed in which the viscous diffusion and convection are treated one after the other. The random walk technique is used for simulation of viscous diffusion. The boundary-layer velocity profile is calculated at one station and compared with theoretically obtained profile.

The second part of the thesis is the simulation of the flow past a bluff body using the full-vortex cloud modelling by the surface vorticity boundary integral method. It develops a discrete vortex element model wherein the body is represented by a number of discrete vortex panels. The strengths of the vortices are related directly to the tangential velocity outside the boundary-layer. Finally the drag and lift coefficients are calculated by getting pressure distribution on the surface of the body and compared with the available data. We get good representation of the nature of the wake but the pressure calculation suffer from too much numerical noise.

In the last part of this thesis an attempt is made to develop a procedure for calculating the flow past multiple two-dimensional bodies. The assembly technique of two mutually interacting bodies is found to be encouraging. We got the satisfactory vortex cloud solution for various Reynolds numbers. The main disadvantage in this method is that there is a lot of numerical noise in pressure calculation in unsteady flow, and the results are not yet satisfactory.

Acknowledgements

I would like to place on record my gratitude to my advisor Dr. Vijay Gupta, Professor, Department of Aerospace Engineering, I.I.T. Kanpur. His encouraging attitude has been of immense help during my M.Tech. program.

Finally, I thank to my parents and my family members for their affection and loving attitude, and, most pleasantly, my special thanks to all my seniors and friends for providing me timely help.

Manish Kumar Jain

M.Tech.(A.E.)

I.I.T.Kanpur

Contents

1	INTRODUCTION	1
1.1	Literature survey	1
1.2	Vortex cloud approach	3
1.3	Shedding of vortices	3
1.4	Body Representation	4
1.5	The Full-Vortex Cloud method	5
1.6	Present work	7
2	SIMULATION OF A BOUNDARY LAYER	8
2.1	Introduction	8
2.2	Solution of the diffusion equation	9
2.2.1	Diffusion of a vortex	11
2.2.2	Random number generation (Step 1)	11
2.2.3	Vortex diffusion over a time steps Δt (Step 2)	12
2.2.4	Radial distribution of vorticity	13
2.3	Discrete vortex simulation of the boundary layer	14
2.3.1	Vorticity creation and shedding (Step 1)	17
2.3.2	Viscous diffusion (Step 3)	17
2.3.3	Vortex convection (Step 5)	18
2.3.4	Merge of vortices in close proximity (Step 6)	20

2.3.5	Calculation of velocity profile (Step 9)	21
2.4	Results and Discussions	21
3	THE FULL-VORTEX CLOUD ANALYSIS OF FLOW PAST BLUFF BODIES	28
3.1	General Introduction	28
3.2	Martensen method	29
3.2.1	Surface element geometry	32
3.2.2	Determination of Coupling coefficients	33
3.3	Martensen analysis in the presence of a cloud of vortices	35
3.4	Vortex shedding from the body surface	36
3.5	Diffusion of vortices	36
3.6	Convection of vortices	37
3.6.1	Convection of vortices in very close proximity to body surface	39
3.7	Zero circulation condition for RHS term	41
3.7.1	Conservation of vortices	42
3.8	Merge and Reflection of the Vortices	43
3.9	Calculation of surface pressure distribution and forces	43
3.10	Determination of Lift and Drag coefficient	44
3.11	Results and discussions	45
4	THE FLOW PAST THE MULTIPLE BODIES	63
4.1	General Introduction	63
4.2	Modification for bodies in close proximity	65
4.3	Results and discussions	66
5	CONCLUSIONS	71

LIST OF FIGURES

Fig. 2.1. Random diffusion of 50 vortex elements over four time steps.

Fig. 2.2. Mirror image system for modelling vorticity creation and convection in discrete vortex simulation.

Fig. 2.3. Laminar boundary layer on a flat plate with constant U

Fig. 2.4. Laminar boundary layer on a flat plate at $Re = 500, 1000$ and 2000

Fig. 2.5. Boundary layer on a flat plate at $Re = 50000$ and 100000

Fig. 2.6. Discrete vortex prediction of flat plate turbulent boundary layer at $Re = 50000$ and 100000

Fig. 3.1. Discrete surface vorticity model for a 2-D body.

Fig. 3.2. Surface element geometry.

Fig. 3.3. Self-induced velocity of a surface vorticity element.

Fig. 3.4. Mirror image system for self-induced convection.

Fig. 3.5. Full vortex cloud solution for circular cylinder at $Re = 20000$

Fig. 3.6. Full vortex cloud solution for circular cylinder at $Re = 30000$

Fig. 3.7. Full vortex cloud solution for circular cylinder at $Re = 40000$

Fig. 3.8. Full vortex cloud solution for circular cylinder at $Re = 50000$

Fig. 3.9. Lift and drag coefficients on a circular cylinder at $Re = 20000$

Fig. 3.10. Lift and drag coefficients on a circular cylinder at $Re = 30000$

Fig. 3.11. Lift and drag coefficients on a circular cylinder at $Re = 40000$

Fig. 3.12. Lift and drag coefficients on a circular cylinder at $Re = 50000$

Fig. 3.13. Full vortex cloud solution for square cross section at $Re = 20000$

Fig. 3.14. Full vortex cloud solution for square cross section at $Re = 30000$

Fig. 3.15. Full vortex cloud solution for square cross section at $Re = 40000$

Fig. 3.16. Full vortex cloud solution for square cross section at $Re = 50000$

Fig. 3.17. Lift and drag coefficients on a square cross section at $Re = 20000$

Fig. 3.18. Lift and drag coefficients on a square cross section at $Re = 30000$

Fig. 3.19. Lift and drag coefficients on a square cross section at $Re = 40000$

Fig. 3.20. Lift and drag coefficients on a square cross section at $Re = 50000$

Fig. 4.1. Flow past a square in close proximity of a rectangle.

Fig. 4.2. Full vortex cloud solution for two multiple bodies at $Re = 20000$

Fig. 4.3. Full vortex cloud solution for two multiple bodies at $Re = 30000$

Fig. 4.4. Full vortex cloud solution for two multiple bodies at $Re = 40000$

Fig. 4.5. Full vortex cloud solution for two multiple bodies at $Re = 50000$

NOMENCLATURE

U_{∞}	Free stream velocity in the x-direction
V_{∞}	Free stream velocity in the y-direction
W_{∞}	Free stream resultant velocity
t	Time
$dt, \Delta t$	Time step
Γ	Circulation
$\omega(r, t)$	Vorticity distribution in space and time
\mathbf{q}	Velocity vector
ν	Dynamic viscosity
∇^2	Laplacian operator
P_i, Q_i	Random numbers
M	Number of elements or panels
ϵ	Offset
ϕ	Angle
s	Distance around profile
$ds, \Delta s$	Element length
N_t	Convection steps
N_d	Diffusion steps
u_t	Velocity close to the wall
Re	Reynolds number
$\gamma(s)$	Vorticity strength
ρ	Fluid velocity
r_{mn}	Distance vector between m and n vortices
β_n	Slope at element n
$K(s_m, s_n)$	Coupling coefficient
Z	Number of shed vortices
C_p	Surface pressure coefficient
C_l	Lift coefficient
C_d	Drag coefficient
P_0	Stagnation pressure
P	Static pressure
f	Frequency of vortex shedding
St	Strouhal number

Chapter 1

INTRODUCTION

1.1 Literature survey

The postulate by L. Prandtl in 1903 that fluid flows at large values of Reynolds number can be modelled as essentially inviscid with thin regions of viscous activities near the solid boundaries could not be used with profit in flow about bluff bodies, where the separation of these thin regions of viscous flow, termed as boundary layers from the solid surfaces disturbed the flow rather drastically. Consequently, the inviscid methods which depended upon the fact that regions of viscous flows were thin and close to the body and the pressure variations across them was negligible, could not be of much use in the calculation of flow about the bluff bodies. The discrete-vortex methods are a class of methods that retain the chain and simplicity of the inviscid method, and yet are able to account for the development of wake behind bluff bodies. The discrete-vortex methods have evolved slowly and have built upon the concepts introduced by various researchers.

Theodore Von Karman had shown in 1911 that at relatively low values of Reynolds numbers the wake behind a bluff body consists of a series of vortices, which are shed alternately from the two separation points, one on either side of the body, and

convected downstream with the fluid. It was natural to explore the dynamics of such vortices and to exploit it for predicting the flows about bluff bodies. Helmholtz has shown earlier in 1858 that in an inviscid flow, vortex lines are material lines, i.e. they are continually composed of the same fluid particles, and that flows with vorticity can be modelled with vortices of appropriate circulation and infinitesimal cross-section. It was this realization which later led to the discretization of compact regions of vorticity into a number of lines or points vortices embedded within potential flows.

Rosenhead (1931) is generally recognized to be the first person to use this approach to study the problem of Kelvin-Helmholtz instability of vortex sheets. He discretized a vortex sheet into a number of discrete vortices and allowed these vortices to convect under mutual influence after an initial sinusoidal perturbations. After a number of time steps, the vortex roll up along the sheet developed, culminating finally in a simple row of vortex bunches, very similar to half of a von Karman vortex sheet.

After the success of Rosenhead, Abernathy and Kronauer (1962) extended this method to modelling the alternating vortex shedding in the wake of the circular cylinder by considering the stability of two parallel vortex sheets. Under the self-convection superposed on a free-stream velocity, the Karman sheet like pattern soon evolves. Abernathy and Kronauer concluded that the role of the bluff body is not very important in the formation of the characteristic vortex street except in its function as a source of the vortex sheet.

There has been a large number of studies which have used various schemes to solve a large variety of problems. The excellent reviews by Clements and Maull (1975), Saffman and Baker (1979), Saffman (1981), Leonard (1980) and Sarpakaya (1989) summarized the activities of several groups. Much of the physical insights into the phenomenon of vortex shedding that has formed the basis of the vortex methods have been reviewed by Windhall (1975) and Mair and Maull (1971).

1.2 Vortex cloud approach

The method of vortices consists of introducing in an essentially potential isolated vorticity elements (of various descriptions) which then convect under the superposed potential flow and the mutual influence of the vortices which can be predicted by Biot - Savart law or Green's function method. The vorticity elements are tracked numerically using Lagrangian (or mixed Lagrangian - Eulerian) Schemes.

1.3 Shedding of vortices

The application of discrete vortex method to separated flow about bluff bodies requires that modelling of the separating vortex sheet, and its discretization. In general, two classes of methods can be identified those involving separation at fixed position in which the location of separation points is allowed to be determined by some condition.

Clement (1973) and Kiya and Arie (1977, 1988) preferred the use of fixed nascent vortex position, where new vortices appear periodically in time at fixed spatial locations close to the experimentally known separation points. The rate of vorticity generation is obtained from the shear layer velocity U_s at these points.

$$\frac{\partial \Gamma}{\partial t} = 0.5 U_s^2 \quad (1.1)$$

This formulation is sought to be justified from the pioneering work of Fage and Johansen (1928) on structure of vortex sheets. Kiya and Arie (1977) carried out a parameteric evaluation of the variations of the location of these nascent - vortex location points and compared the calculated results with those obtained experimentally to fix a proper location.

Sarpakaya (1989) refers to a work of Kuwahara (1973) wherein he determines the strengths of the nascent vortices appearing at fixed locations by using the Kutta

conditions. Kuwahara is reported to have found that the amplitude of the normal force coefficient calculated in this manner depends very strongly upon the assumed position of the two fixed points where the nascent vortices appear. In fact, a small change in the position of nascent vortices is reported to cause an eight - fold change in the normal force coefficient.

In these methods, no interaction is allowed between the shed vortices and the appearance of the nascent vortices. Thus, the velocities at the outer edges of the shear layer are only indirectly related to the strength of the vortex and the fixed time interval. Evidently, the velocities in the inner and the outer edges of the shear layer, the strength and position of the nascent vortices, and the Kutta condition are interdependent and, therefore, the location and time interval cannot be chosen arbitrary.

Sarpakaya (1975) introduced a procedure wherein he used variable nascent-vortex positions using Kutta condition. Parag Kumar (1993), using the lead provided by Sarpakaya based the strength of the nascent vortices on

$$\frac{\partial \Gamma}{\partial t} = 0.5 U_{s,m}^2 \quad (1.2)$$

where $U_{s,m}$ is the mean velocity of the shear layer calculated using the average of the convective velocities of the first four vortices in each shear layer. This appears to provide a satisfactory mechanism for feedback to the rate at which the vorticity is shed.

1.4 Body Representation

For calculating flows past bodies, the vortex methods, like all other inviscid methods, require that the flow tangency condition be satisfied. The no-slip condition is another matter and will be discussed later.

For many 2-D geometries conformal transformation offers a convenient method for satisfying the tangency condition. For a circular cylinder a simple transformation and the use of circle theorem yields one image per vortex at the inverse point. For a cylinder of arbitrary cross-section Sarpakaya (1975), Clement and Maul (1975) used Shwartz- Christoffel transformation, Shoff and Franks (1981) used truncated Laurent series, and Parag Kumar(1993) used a Zukowsky transformation for calculating flow past a flat plate at various angles of attack.

The use of conformal transformation for 2-D geometries involve repeated transformation from physical plane to circular plane and to W-plane for velocities must be calculated in the W-plane but the convection of vortices must be calculated in the physical plane. Further Routh rule needs to be used to calculate correctly the velocity in the physical plane. (see Milne Thompson (1969), Clements (1973a, 1973b, 1977) and Sarpakaya (1968).

Another approach at body representation uses surface singularity sheets, most notably vortex sheets. Any potential solution ϕ can be expressed, following Greens Theorems, as the sum of the influences of the boundary singularity sheets. The resulting integral equation is discretized into a set of algebraic equations and solved numerically for the set of panel strengths (sources, doublet or vortices) by enforcing the tangency boundary condition at the finite number of collocation points (Smith (1962), Smith and Hess (1966), Hunt (1978), Lewis (1981, 1987)).

1.5 The Full-Vortex Cloud method

A relatively recent development is the so-called 'full-vortex cloud' modelling which attempts to simulate the flow through the a solution of Navier-Stokes equation by an operator- splitting method , first proposed by Chorin (1973,1978). It has been developed extensively by Smith and Stansby (1987), Lewis and Porthouse (1981)

and Porthouse(1983).

In this method, the vorticity equation is divided into a convective and and diffusive part and two equations are solved sequentially.

Thus, the Navier-Stokes equation

$$\frac{\partial \mathbf{q}}{\partial t} + \mathbf{q} \cdot \nabla \mathbf{q} = -\frac{\nabla p}{\rho} + \nu \nabla^2 \mathbf{q} \quad (1.3)$$

is first converted into the two dimensional vorticity transport equation

$$\frac{\partial \omega}{\partial t} + \mathbf{q} \cdot \nabla \omega = \nu \nabla^2 \omega \quad (1.4)$$

and then is split into two equations

$$\frac{\partial \omega}{\partial t} + \mathbf{q} \cdot \nabla \omega = 0 \quad (1.5)$$

and

$$\frac{\partial \omega}{\partial t} = \nu \nabla^2 \omega \quad (1.6)$$

or its non-dimensionalized version

$$\frac{\partial \omega}{\partial t} = \frac{1}{\text{Re}} \nabla^2 \omega. \quad (1.7)$$

The two equations are then solved sequentially. A practical manifestation starts with the potential flow about the body calculated with vortex sheet replacing the body surface. This vortex sheet is then discretized into a number of vortices. The vortices are then made to diffuse according to equation 1.6 by using some kind of random-walk technique. After the diffusive step, the vortices are then allowed to convect with the convection velocity determined by the influence of all the vorticity elements, the free stream and the new vortex sheet required to satisfy the tangency boundary condition. After convection, the tangency condition is satisfied again, and the new sheet is ready to be shed, diffused and convected.

1.6 Present work

The present work is in essence an extension of the work started by Parag Kumar (1993) and continued by Verma (1994). Parag Kumar calculated the flow past an inclined flat plate where the body representation was obtained through conformal transformation, and the nascent vortices were shed at points whose location was obtained through Kutta condition and whose strength was based on the shear-layer velocity obtained as the average convection velocity of the first four vortices in the wake immediately next to the plate.

Due to obvious limitation of this scheme in more complicated geometries Verma (1994) adopted a vortex panel scheme for body representation. The vortices were shed from fixed separation points and the angle of the separation streamlines was optimized through trial and error. Verma calculated the flow past a half cylindrical cup facing the flow representing a rather guide 2-D canopy. Verma also started, work on an operator-splitting technique for solving the Navier-Stokes equation and obtain some elementary solutions for flow past a cylinder.

The present work takes off from the work of Verma and develops further the full-vortex cloud scheme involving operator-splitting. The first part of the work is concerned with exploration of the method as applied to the problem of boundary layer on a flat plate. This problem affords the opportunity to explore the problem of large Reynolds number flows and the use of distinct time steps for diffusion and convection.

Next the full-vortex cloud analysis is developed for the problem of flow past a cylinder. The focus of the program was to develop, if possible, the capability to predict drag on bluff bodies with a view to evaluate changes in shapes intended for drag reduction. For this purpose, attempts have been made to develop a procedure for calculating the flow past multiple two-dimensional objects.

Chapter 2

SIMULATION OF A BOUNDARY LAYER

2.1 Introduction

As a preliminary to the development of full-vortex cloud method of calculating the viscous separating flow past a bluff body, let us first consider the computation of the development of a boundary layer on a flat plate by a discrete vortex method.

The vorticity transport equation for the case of incompressible 2-dimensional flow is obtained by taking the curl of the Navier-Stokes equation to obtain

$$\frac{\partial \omega}{\partial t} + \mathbf{q} \cdot \nabla \omega = \nu \nabla^2 \omega \quad (2.1)$$

where the vorticity intensification term $\omega \cdot \nabla \mathbf{q}$ has dropped out because of the two-dimensionality of the flow.

In its non-dimensional form, this becomes

$$\frac{\partial \omega}{\partial t} + \mathbf{q} \cdot \nabla \omega = \frac{1}{\text{Re}} \nabla^2 \omega \quad (2.2)$$

where Re stands for the Reynolds number.

It is convenient to consider the flow past a flat plate (see Fig. 2.2) as a potential flow in which the no slip condition at the plate surface modelled as a source of vorticity there.

The vorticity thus introduced into the flow then diffuses and convects according to the Eqn. 2.2 above. We will develop here the operator-splitting method which was first developed by Porthouse and Lewis(1981) in which the convection and diffusion instead of acting simultaneously are made to act serially, so that equation 2.2 is split into two equations

$$\frac{\partial \omega}{\partial t} = -\mathbf{q} \cdot \nabla \omega \quad (2.3)$$

and

$$\frac{\partial \omega}{\partial t} = \frac{1}{\text{Re}} \nabla^2 \omega \quad (2.4)$$

Equation 2.3 is quite straight formed to handle, on reorganization, one obtain

$$\frac{\partial \omega}{\partial t} + \mathbf{q} \cdot \nabla \omega = \frac{D\omega}{Dt} = 0 \quad (2.5)$$

This is taken to imply that the discretized vortex elements in the flow are convected as material elements at the local flow velocities.

Equation 2.4, which is the classical diffusion equation is solved using a random-walk method, We first develop an algorithm to solve this equation after the procedure suggested by Chorin(1973).

2.2 Solution of the diffusion equation

Batchelor(1970) obtained the well known solution of the problem of diffusion of a concentrated vortex of strength Γ which is located at the origin at time $t = 0$. The subsequent distribution of vorticity in time and space is obtained as

$$\omega(r, t) = \frac{\Gamma}{4\pi\nu t} e^{-\frac{r^2}{4\nu t}} \quad (2.6)$$

which represents the radial distribution of vorticity. Lewis(1981) solved the same problem by discretizing the concentrated vortex into a large number N of vortex elements at time $t = 0$, all located at the origin, and then letting the various elemental vortices undergo a random walk. The strength of each of these elemental vortices is taken as Γ/N .

If the solution after time t is given by Eqn 2.6, then the number n of elemental vortices in an area $r d\theta dr$ at that time should be given by

$$\frac{n\Gamma}{N} = \omega(r, t) r d\theta dr = \frac{\Gamma}{4\pi\nu t} e^{-\frac{r^2}{4\nu t}} r d\theta dr \quad (2.7)$$

If p denotes the probability that a specific element ends up in this area element after time t , then

$$p = \frac{n}{N} = \frac{1}{4\pi\nu t} e^{-\frac{r^2}{4\nu t}} r d\theta dr \quad (2.8)$$

An appropriate random-walk method then displaces each element i in the radial and angular direction by amounts r_i and θ_i over the time interval 0 to t , such that the radial probability distribution given by Equation 2.8 is satisfied for all $r \Delta\theta \Delta r$ elements which make up the given target area.

The angular symmetry of the governing diffusion equation suggests that the scattering in the θ direction should taken place such that an element has equal probability of ending up in any direction. This is achieved by generating a random-walk Q_i between 0 to 1, and letting the element take up

$$\theta_i = 2\pi Q_i \quad (2.9)$$

at the i_{th} time steps.

To obtain the radial scattering of vortex elements first integrate Eqn 2.8 for θ between 0 and 2π and to obtain the probability that a given element will lie between r and $r + dr$, by

$$p = \frac{1}{2\nu t} e^{-\frac{r^2}{4\nu t}} r dr \quad (2.10)$$

This equation may next be integrated over dr for r between 0 and r to obtain the following equation

$$P = 1 - e^{-\frac{r^2}{4\nu t}} \quad (2.11)$$

where P gives the probability that the given vorticity element will lie somewhere within the circle of radius r .

At this point it is interesting to notice that this probability agrees with the normal distribution curve of statistical theory. For the random-walk process, then we generate a random number P_i between 0 to 1 with uniform distribution, Then we postulate that the i th vortex element will be found at a radius r_i such that

$$P_i = 1 - e^{-\frac{r_i^2}{4\nu t}} \quad (2.12)$$

The radial shift of each of the vorticity element can then be obtained if the above equation is inverted as follows

$$r_i = \sqrt{4\nu t \ln\left(\frac{1}{P_i}\right)} \quad (2.13)$$

2.2.1 Diffusion of a vortex

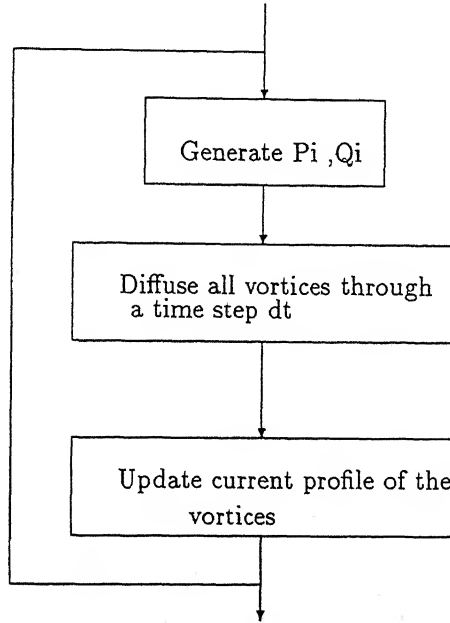
Consider a vortex of strength 1.0 situated at the origin. To obtain the vortex diffusion with time, we implement the above scheme in the manner shown in the flow diagram which is shown on the next page,

2.2.2 Random number generation (Step 1)

Random numbers P_i and Q_i are generated by using formula.

$$P_i = P_{i+1} - \text{integer}(\exp(5.0 \ln(P_{i+1} + 1.10318))) \quad (2.14)$$

by defining a series of annular bins separated by equally spaced the process, e.g. $P = 0.5$. The quality of random number has been verified by using statistical methods.



2.2.3 Vortex diffusion over a time steps Δt (Step 2)

Now consider the diffusion over a small time increment Δt . The displacements of element i during time Δt will then be

$$\Delta\theta_i = 2\pi Q_i \quad (2.15)$$

$$\Delta r_i = \sqrt{4\nu\Delta t \ln\left(\frac{1}{P_i}\right)} \quad (2.16)$$

Thus after the increment Δt the new coordinate location as the i^{th} element will become

$$x'_i = x_i + \Delta r_i \cos \Delta\theta_i \quad (2.17)$$

$$y'_i = y_i + \Delta r_i \sin \Delta\theta_i \quad (2.18)$$

2.2.4 Radial distribution of vorticity

The evaluation of vorticity for the scattered vortex elements, the process, e.g. $P = 0.5$, radius r_j . Suppose that n_j elements are captured by the area lying between r_j and r_{j+1} . Thus, the vorticity at the j th strip will be estimated by

$$\omega(r) = \frac{n_j}{N\pi(r_{j+1}^2 - r_j^2)} \quad (2.19)$$

For example, a unit strength vortex which was represented by 1000 elements of strength 0.001 and kinematic viscosity was 1.0, is given 10 random-walk over the time period $t = 1.0$ based upon the equation (2.15 to 2.18). The output including the comparison with the exact solution has been given in Table 2.1.

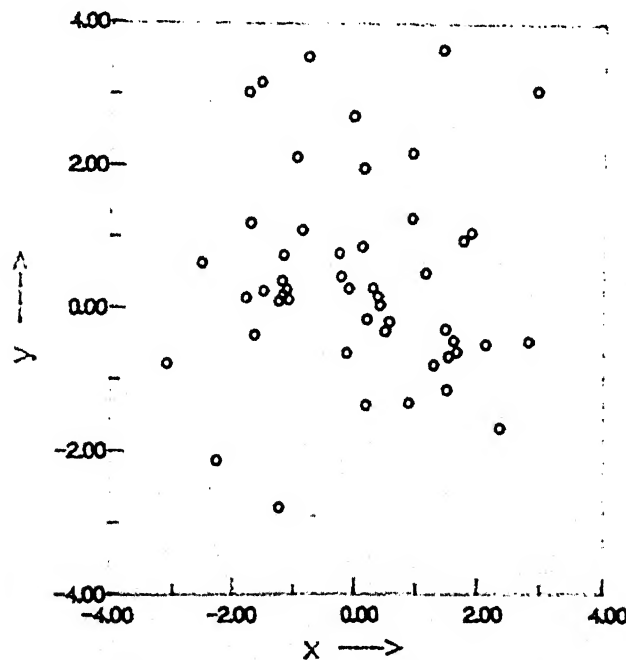


Fig 2.1. Random diffusion of 50 vortex elements over four time steps.

Table 2.1. Diffusion of a point vortex

<i>Bin no.</i>	<i>No. of elements in bin</i>	<i>rms rad.</i>	<i>Numerical soln.</i>	<i>Exact soln.</i>
1	43	0.282843	0.085546	0.078002
2	110	0.632456	0.072946	0.072005
3	157	1.019804	0.062468	0.061358
4	181	1.414214	0.051441	0.048266
5	163	1.811077	0.036031	0.035048
6	125	2.209072	0.022607	0.023494
7	100	2.607681	0.015303	0.014537
8	48	3.006659	0.006366	0.008304
9	36	3.405877	0.004213	0.004379
10	21	3.805260	0.002199	0.002131
11	5	4.204759	0.000474	0.000958
12	10	4.604346	0.000865	0.000397
13	1	5.003998	0.000080	0.000152
14	0	5.403702	0.000000	0.000054
15	0	5.803447	0.000000	0.000018
16	0	6.203225	0.000000	0.000005
17	0	6.603030	0.000000	0.000001
18	0	7.002857	0.000000	0.000000
19	0	7.402702	0.000000	0.000000
20	0	7.802564	0.000000	0.000000

2.3 Discrete vortex simulation of the boundary layer

When a fluid motion is started impulsively from rest, vorticity is generated on the surfaces of all solid boundaries within the flow. From that moment on the viscosity

in the fluid gives rise to viscous diffusion of the vorticity in a direction normal to the surface of the body. If the surface vorticity is divided into discrete elements which are given random motions to simulate viscous diffusion and are subjected to convective influence of the free stream and all other vortices present in the flow, it would appear that a method is immediately available for calculating the development of a boundary layer flow.

But the convection should be handled in a manner which models the presence of the flat plate as in the previous boundary correctly. This is handled here by introducing in the flow field mirror images about $y = 0$ of all the vortices present in the flow. The next effect of the presence of the image system with the system of the physical vortices is to make $y = 0$ a streamline (with zero normal velocity everywhere) and this is what is sufficient for maintaining the boundary condition. Fig. 2.2 shows an appropriate convection scheme based on the operator-splitting procedure discussed above

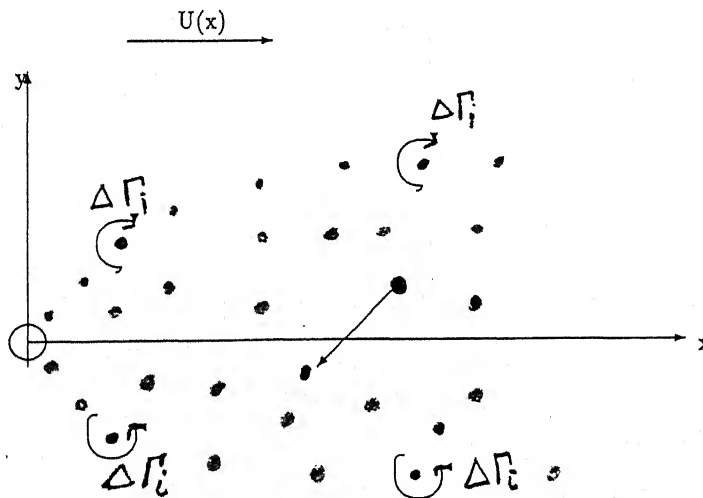
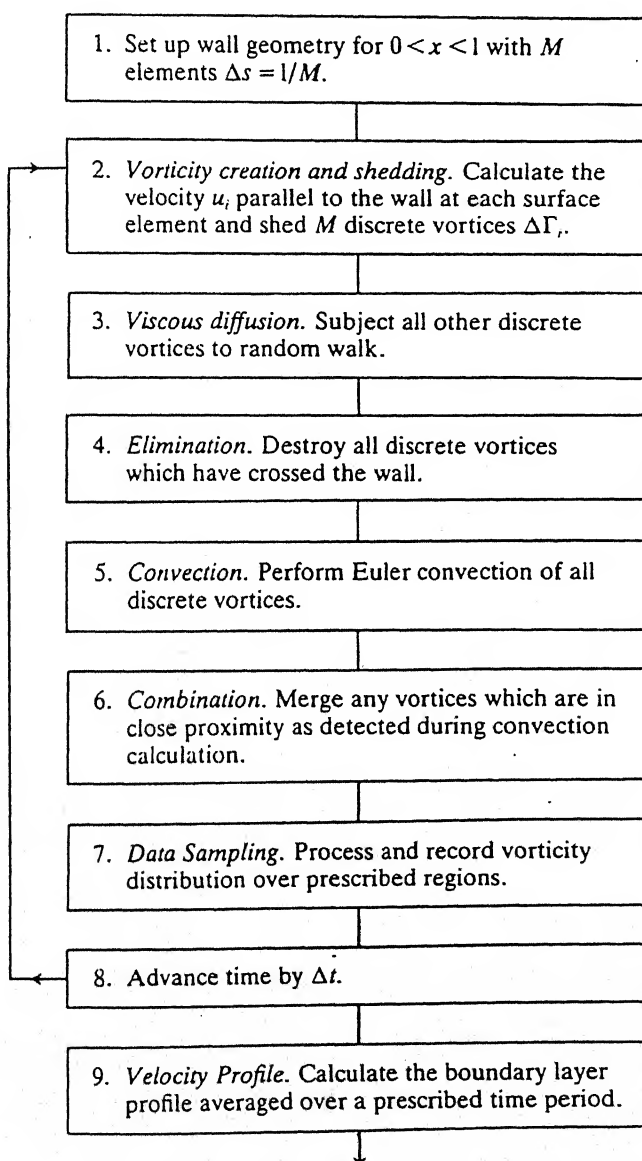


Fig. 2.2. Mirror image system for modelling vorticity creation and convection in discrete vortex boundary layer simulation.

The procedure is based on creating and shedding at the plate surface $y = 0$ a vortex sheet, of discretizing this vortex sheet into a number of line vortex elements,

and then to diffuse and convect. These vortices and other vortices are in the flow field appropriately. At each time step, the number of vortices are introduced at the plate surface. The development of the steady boundary-layer is then achieved through an unsteady process.



2.3.1 Vorticity creation and shedding (Step 1)

According to the fundamental principle of the vortex-sheet method, the strength of the vortex sheet that needs to be postulated at a surface is equal to the slip velocity at that surface under the action of the inviscid potential flow and the vortices that have been shed up to that time.

Thus, at time $t = 0$, the slip velocity is U all along the flat plate and the initial vortex strength is $\gamma(s_i) = U$ at $y = 0$ all along the wall surface $0 < x < l$. Due to viscosity this sheet will immediately begin to diffuse in the manner discussed in section 1.2, and also undergo convection. At any later time, the new vortex sheet at the plate will have strength given by

$$\gamma(s_i) = u_i = U - \frac{1}{\pi} \sum_{j=1}^N \frac{\Delta\Gamma_j y_j}{(x_i - x_j)^2 + y_j^2} \quad (2.20)$$

where $\Delta\Gamma_j$ is the strength of the discrete vortex j in the flow field (shed previously) and located currently at (x_j, y_j) .

This vorticity is shed freely from the surface and is represented by M new discrete vortices of strength $\Delta\Gamma_i = \gamma(s_i)\Delta s_i$, now free to undergo diffusion and convection.

In calculating the slip velocity, the summation in Equation 2.19 has to be carried out over all vortices and their mirror images, which are introduced to take care of the normal velocity boundary condition.

2.3.2 Viscous diffusion (Step 3)

After the creation and shedding of the new vorticity, all other discrete vortices must be subjected to random walks to simulate viscous diffusion during the time step Δt . A complication that results in this procedure that about half the newly created vortices, and some of the other vortices, diffuse to the half region $y < 0$. This clearly is unacceptable because of the impervious wall boundary condition. Chorin (1978) used a scheme in which he started with a double strength $2\gamma(s_i)\Delta s_i$ with about

one half of the vortices that are diffused under the plate being simply quenched. This results in about the right amount of vorticity being introduced in the flow.

Porthouse (1983) recommended that the nascent vortices may be introduced at an offset from the wall. Based on the consideration of the root mean squared development of vorticity, he recommended a displacement $\epsilon = \sqrt{4\nu\Delta t/3}$.

We have used the Porthouse recommendation and in addition used a reflection procedure interior of the body (below the plate $y = 0, 0 < x < l$ in this present case of the flat plate) is reflected back normally the same distance. This conserves the vorticity in the diffusion as well as the convection operation.

2.3.3 Vortex convection (Step 5)

As we have noticed the governing equation for the vortex convection phenomenon is

$$\frac{\partial \omega}{\partial t} + \mathbf{q} \cdot \nabla \omega = 0 \quad (2.21)$$

A numerical simulation of this equation suitable for computation is possible if a large number of point vortices are taken to simulate the area distribution of vorticity within a given region of the flow. Each element will then move under the influence of all the other elements. Vortex convection in this simple geometry of flat plate is correctly modelled by the mirror image system as shown in Fig 2.2. The convection velocity components experienced by element $\Delta\Gamma_j$ due to element $\Delta\Gamma_i$ and its mirror image are then given by

$$\Delta u_j = \frac{\Delta\Gamma_i}{2\pi} \left(\frac{y_j - y_i}{r_1^2} - \frac{y_j + y_i}{r_2^2} \right) \quad (2.22)$$

$$\Delta v_j = \frac{\Delta\Gamma_i}{2\pi} (x_j - x_i) \left(\frac{1}{r_2^2} - \frac{1}{r_1^2} \right) \quad (2.23)$$

where,

$$r_1^2 = (x_j - x_i)^2 + (y_j - y_i)^2 \quad (2.24)$$

$$r_2^2 = (x_j - x_i)^2 + (y_j + y_i)^2 \quad (2.25)$$

$$(2.26)$$

Now, we can sum up the influence of all the vortices in the cloud as

$$U_{j,cloud} = \sum_{\substack{i=1 \\ i \neq j}}^{i=N} \frac{\Delta \Gamma_i}{2\pi} \left(\frac{y_j - y_i}{r_1^2} - \frac{y_j + y_i}{r_2^2} \right) \quad (2.27)$$

$$V_{j,cloud} = \sum_{\substack{i=1 \\ i \neq j}}^{i=N} \frac{\Delta \Gamma_i}{2\pi} (x_j - x_i) \left(\frac{1}{r_2^2} - \frac{1}{r_1^2} \right) \quad (2.28)$$

In addition to this we have the self-induced velocity of element $\Delta \Gamma_i$ obtained through the effect of its mirror image vortex.

$$\Delta u_i = -\frac{\Delta \Gamma_i}{4\pi y_i}, \quad \Delta v_i = 0 \quad (2.29)$$

The resultant velocity of the i^{th} vortex is simply given by the combined influence of all the terms and the external velocity.

$$u_i = U_{i,external} + U_{i,cloud} + \Delta u_i \quad (2.30)$$

$$v_i = V_{i,external} + V_{i,cloud} \quad (2.31)$$

Applying a forward difference for the elementary time step Δt the new position of the vortex is then computed from

$$x'_i = x_i + u_i \Delta t \quad (2.32)$$

$$y'_i = y_i + v_i \Delta t \quad (2.33)$$

Since all irreversibilities arise because of viscous diffusion which is not included in this step, the convective algorithm is developed so that it is completely invisible. This has been ensured by using a multi-step prediction-correction scheme.

2.3.4 Merge of vortices in close proximity (Step 6)

Though the discrete vortex model gives fairly good representation of the flow fields, the nature of modelling in which region of viscous flow with vorticity are replaced by inviscid free vortices, with velocities tending to infinite as one approaches the line vortex, makes the flow field close to a vortex to be highly vortex. This results in the convection velocities of vortices close to other vortices to be insignificant and random errors.

Various schemes have been tried to overcome this problem, and all of them depends upon smudging a point vortex into a vortex blob, and any blobs which touch one-another are merged algebraically.

We have developed a procedure in which each newly created sheet vortex element of strength $\gamma(s_i)$ and element length Δs_i is immediately redistributed as a Rankine vortex of radius $r_0 = \Delta s_n / \pi$ for which the induced velocity at radius r is given by

$$\Delta q = \frac{\Delta \Gamma r}{2\pi r_0^2} \text{ for } r < r_0 \quad (2.34)$$

$$= \frac{\Delta \Gamma}{2\pi r} \text{ for } r > r_0 \quad (2.35)$$

Any vortices which drift close enough for their vortex cores to be overlapping are then merged into a single vortex and the resultant strength of the vortices will be algebraic sum of the individual vortices and it will be placed at the center of vortices. For example two vortices of strength Γ_1 and Γ_2 located at positions (x_1, y_1) , (x_2, y_2) which happen to be closer to one another than a specified limit r_{min} , which is equal to the sum of the radius of the two interacting Rankine vortex.

Thus, vortices which are drifted closer than the r_{min} are merged into a single vortex and after merging the two vortices the strength of the resulting vortex is given by

$$\Gamma = \Gamma_1 + \Gamma_2 \quad (2.36)$$

at the position

$$x = \frac{|\Gamma_1| x_1 + |\Gamma_2| x_2}{|\Gamma_1| + |\Gamma_2|} \quad (2.37)$$

$$y = \frac{|\Gamma_1| y_1 + |\Gamma_2| y_2}{|\Gamma_1| + |\Gamma_2|} \quad (2.38)$$

The combination produces two results. First it ensures that unrealistically large convection velocities are not introduced, and second, that the total number of vortices in the field remains manageable.

2.3.5 Calculation of velocity profile (Step 9)

The velocity profile is calculated by integrated the vorticity profile, neglecting the velocity component v in the y direction, which is a standard boundary -layer theory assumption. Thus,

$$u(y) = \int_0^y \omega(y) dy \quad (2.39)$$

Numerically, the $\omega(y)$ profile is obtain by establishing at the required location x , sampling boxes of width Δx and height Δy spacing the total number of vorticity elements present in each boxes at a given time step are counted, and then $\omega(y_i)$ is obtained by dividing the box at height y_i by its area $\Delta x \Delta y$

Then, the velocity at y_n is obtained by

$$u(y_n) = \int_0^{y_n} \omega(y) dy \quad (2.40)$$

$$\approx \sum_{i=1}^n \omega(y_i) \Delta y \quad (2.41)$$

2.4 Results and Discussions

A typical vortex cloud, due to the scatter of vorticity elements, as it develops on the flat plate is shown in Fig 2.3. 60 surface elements were used to represents a plate of length $l = 1.0$ with a uniform mainstream flow at $U = 1.0$ Fig. 2.4. shows the

velocity profile as obtained by the above scheme for Re 500, 1000 and 2000. The Blasius profile is also shown in the figures for comparison.

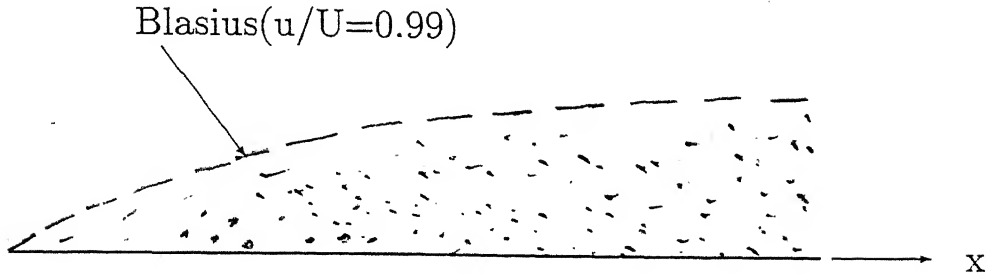


Fig 2.3. Laminar boundary layer on a flat plate with constant mainstream velocity U

Selection of element size and time step

An appropriate device of the time step Δt is one in which the convective and diffusive displacement are of the order of the element size. Thus, the convective displacement δ_c which is of order $\frac{1}{2}U\Delta t_c$ should be of the same order as the element size, say $\frac{l}{2M}$, M being the number of panels taken along the plate. This gives the convective time step as $\Delta t_c \approx \frac{l}{MU}$.

The typically diffusive displacement on the other hand is

$$\Delta r_i = [4\nu\Delta t \ln(\frac{1}{P_i})]^{1/2} \quad (2.42)$$

obtain from Equation 2.25. by as $\delta_d \approx [4\nu\Delta t \ln 2]^{1/2}$, so that

$$\delta_d \approx [4\nu l \ln 2 / MU]^{1/2} \quad (2.43)$$

or

$$\frac{\delta_d}{\frac{l}{2M}} \approx M^{\frac{1}{2}} \left(\frac{4\nu}{Ul} \right)^{\frac{1}{2}} \quad (2.44)$$

$$= \left(\frac{16M}{\text{Re}} \right)^{\frac{1}{2}} \quad (2.45)$$

or

$$\Delta t = \frac{16l \ln 2}{U \text{Re}} \quad (2.46)$$

For very large Reynolds numbers then, we see that the diffuse displacement time step is extremely small. A considerable saving in calculation effort can be effected by choosing different time scales for diffusion and convection.

Thus, with reference to Equation 2.14 , we choose $\Delta t = \Delta t_D$ such that $\delta_D = \frac{l}{2M}$, so that

$$\Delta t_D = \frac{l^2}{16\nu M^2 \ln 2} \quad (2.47)$$

The ratio of the diffusive time step Δt_D to the convective Δt_c then is

$$\frac{\Delta t_D}{\Delta t_c} = N_t = \frac{\text{Re}}{16M \ln 2} \quad (2.48)$$

For a value of $\text{Re} = 10^5$ and $M = 100$, we obtain a value of $N_t = 90$. This means that for each 90 convective steps we need to perform only one diffusive step. This results in a very considerable saving in time of computation.

Fig. 2.5 shows the boundary layer profile generation by vortex dynamics for $\text{Re} = 50000$ and 100000 . At these Reynolds numbers, most boundary layers are still laminar, therefore close to turbulent. But the calculated profile is quite different from the Blasius profile suggested that the numerical turbulence implied by the finite scale $\Delta s/\pi$ of the discrete vortices perturbs the shear layer leading to transition.

Vortices close to walls

The vortices which are too close to wall, develop the boundary-layer velocity profile according to the law of the wall,

$$\frac{u}{u_\tau} = \frac{yu_\tau}{\nu} \quad \text{for } \frac{yu_\tau}{\nu} < 11 \quad (2.49)$$

$$= 2.44 \ln \left(\frac{yu_\tau}{\nu} \right) + 4.9 \quad \text{for } \frac{yu_\tau}{\nu} > 11 \quad (2.50)$$

where the friction velocity u_τ is defined in term of wall shear stress τ_0 by

$$u_\tau = \sqrt{\frac{\tau_0}{\rho}} \quad (2.51)$$

$$= \sqrt{\nu \frac{du}{dy}|_{y_0}} = \sqrt{\nu \omega(y_0)} \quad (2.52)$$

Thus u_τ may be directly related to the vorticity $\omega(y_0)$ close to the wall. The suitable approach here to calculate $\omega(y_0)$ is to take the average vorticity strength over the inner half of the sub-layer. The logarithmic scale of plotting then helps to draw out the characteristics of the boundary layer in both the laminar near wall and turbulent outer regions. The solution for Re (50000 and 100000) has been shown in Fig. 2.6. The results which comes directly from the law of the wall are also incorporated for the comparison.

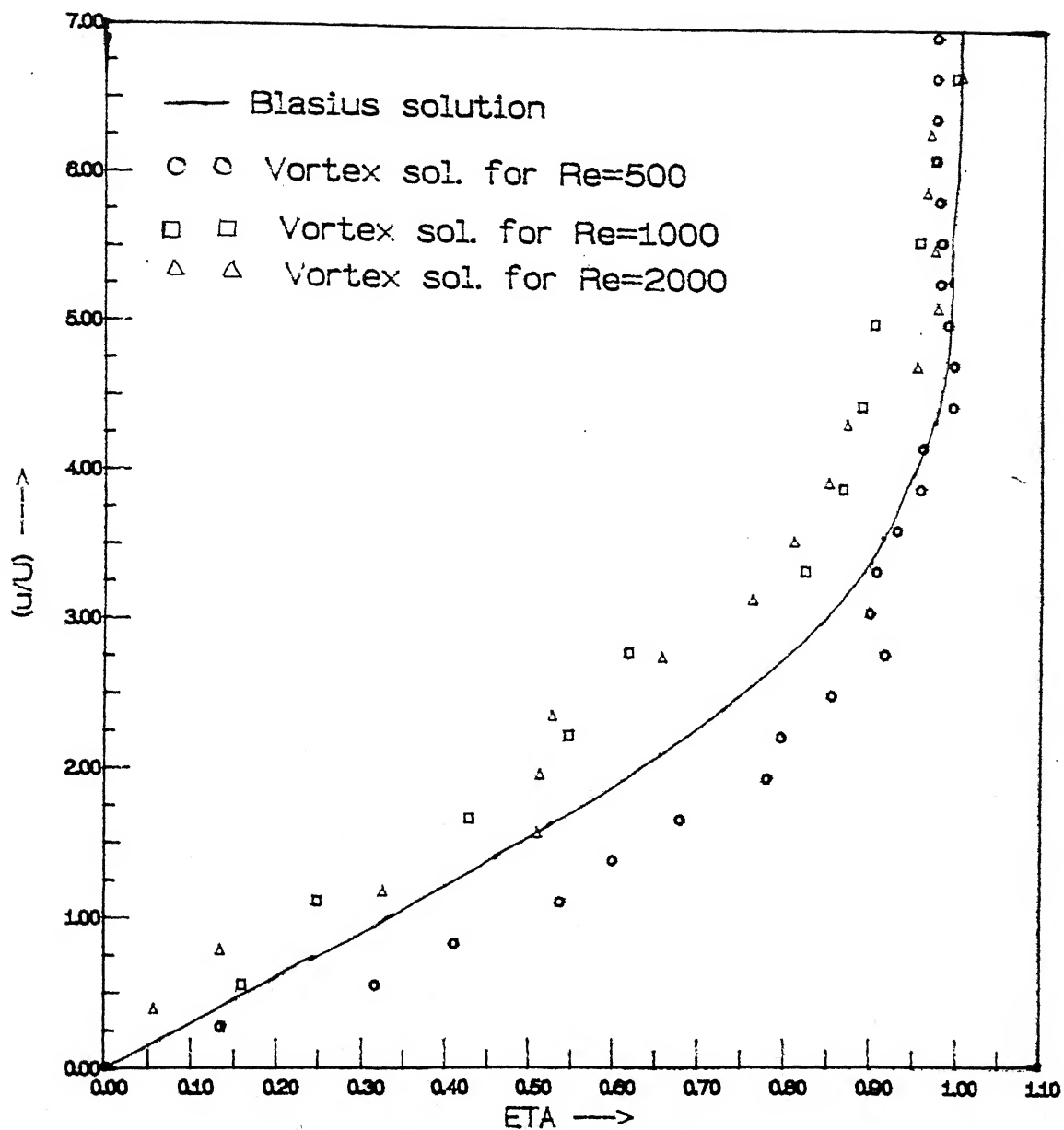


Fig. 2.4. Laminar boundary layer on a flat plate at $Re=500, 1000$ and 2000

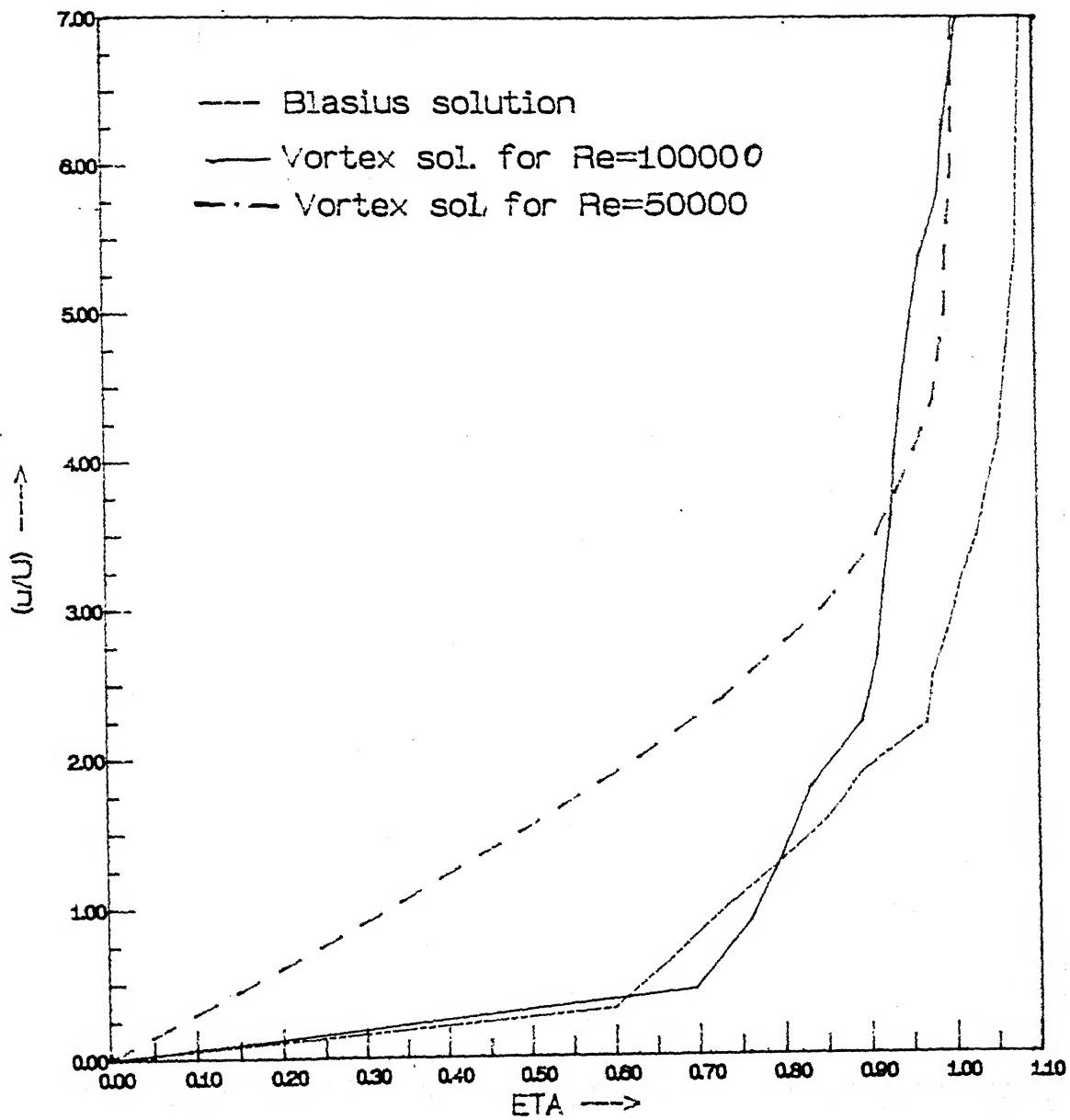


Fig. 2.5. Boundary layer on a flat plate at $Re=50000$ and 100000

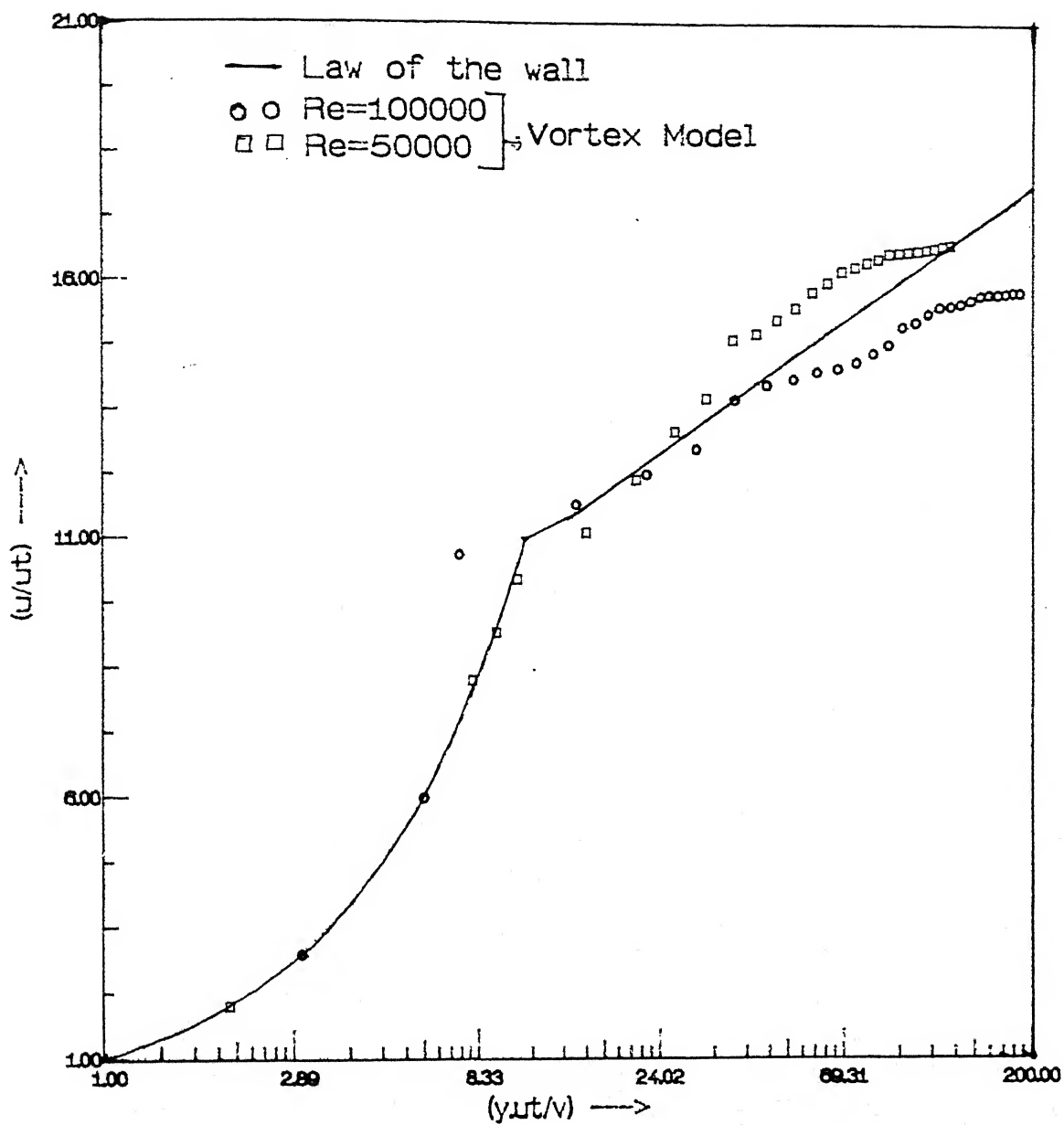


Fig. 2.6. Discrete vortex prediction of flat plate turbulent boundary layer at Re=50000 and 100000

Chapter 3

THE FULL-VORTEX CLOUD ANALYSIS OF FLOW PAST BLUFF BODIES

3.1 General Introduction

In this chapter the method of the full-vortex cloud developed in the last chapter is extended for flow past two-dimensional bodies of arbitrary shapes. The method is an extension of the traditional discrete vortex methods which are valid for infinitely large Reynolds number (though with the postulation of the separated wake), and attempt to include the effect of the finite (but large) Reynolds numbers, and is based essentially on the procedure developed by Verma (1994).

The surface of the two-dimensional body is covered with discretized vortex-panels. The strength of which is determined using Martensen method which is based on satisfying the zero tangential velocity condition by postulating a vortex sheet at the body surface.

Following the treatment developed in the last chapter, this vortex sheet is seen

as the incipient boundary layer, which develops as this vorticity diffuses into the flow field and is convected downstream. The numerical scheme^{is} developed in this chapter. The basic strategy is displayed in the given flow diagram and following the operator splitting procedure developed in the previous chapter.

3.2 Martensen method

Consider the flow past a two-dimensional body of an arbitrary shape in the (x-y) plane, immersed in a uniform flow W_∞ at an angle of attack α_∞ measured with respect to x-axis as shown in Fig. 3.1. We may discretize the body surface into M elements. Let the length of n^{th} panel be ds_n and let it be covered by a vorticity sheet of strength $\gamma(s)$ per unit length. The distance s is measured in the clockwise direction around the body perimeter from some datum which is usually chosen as the leading edge of the body.

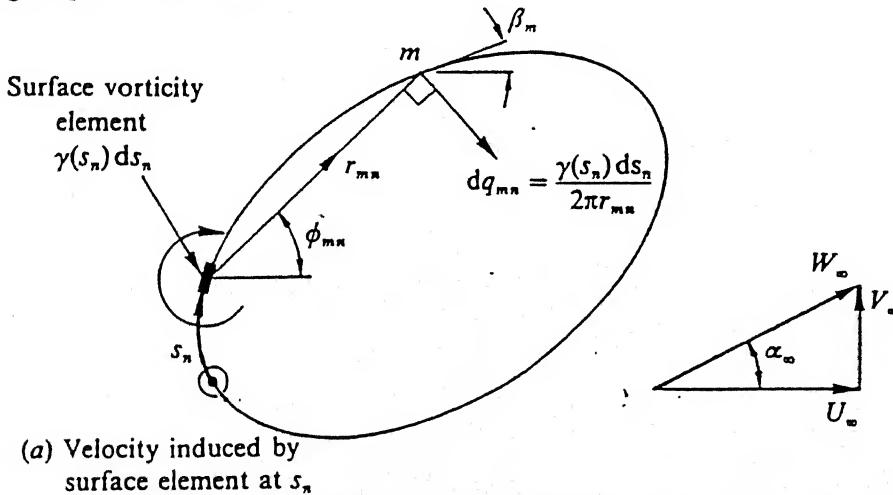
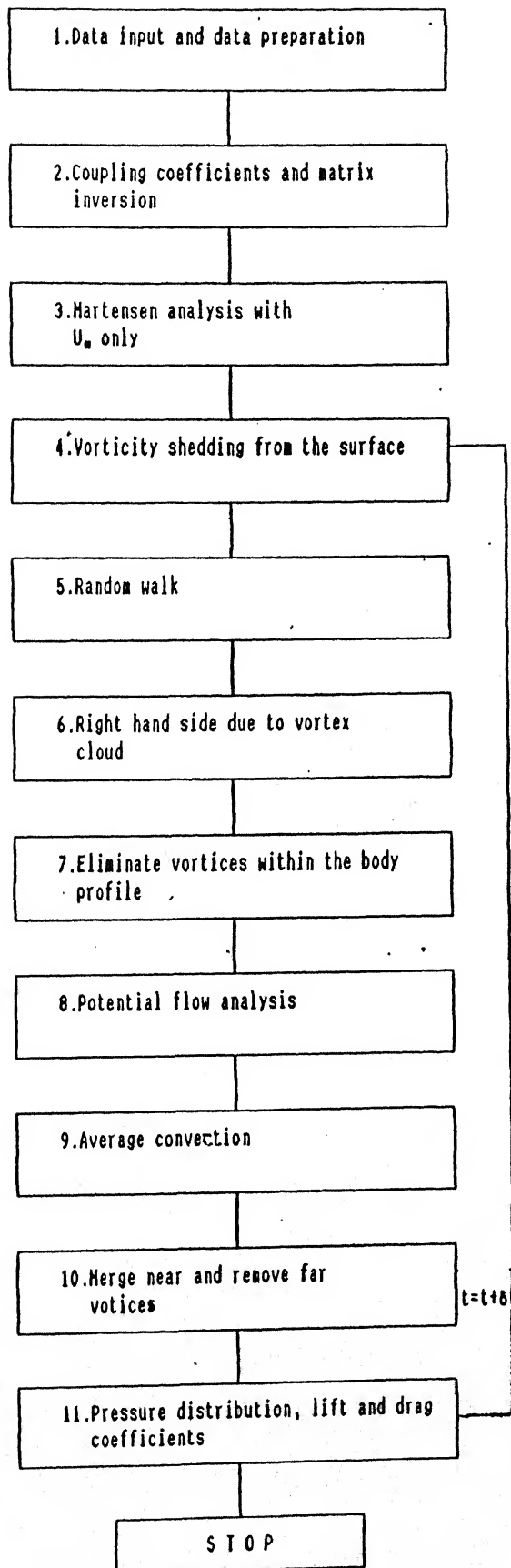


Fig. 3.1. Discrete surface vorticity model for a 2-D body

The velocity dq_{ij} induced at s_i due to a small vorticity element $\gamma(s_j)ds_j$ located at s_j elsewhere on the body directly follows from the Biot-Savart law, which in this



Flow diagram for full vortex cloud analysis.

case reduces to:

$$dq_{ij} = \frac{\gamma(s_j)ds_j}{2\pi r_{ij}} \quad (3.1)$$

where r_{ij} is the distance between the elements i and j . Now resolve dq_{ij} parallel to the body surface at i where the profile slope is expressed as β_i . We express dq_{ij} in terms of local coordinates by introduce a figure here to show coordinates first.

$$dU_{ij} = \frac{\gamma(s_j)ds_j}{2\pi r_{ij}} \sin \phi_{ij} = \frac{(y_i - y_j)}{2\pi r_{ij}^2} \gamma(s_j)ds_j \quad (3.2)$$

$$dV_{ij} = \frac{-\gamma(s_j)ds_j}{2\pi r_{ij}} \cos \phi_{ij} = \frac{-(x_i - x_j)}{2\pi r_{ij}^2} \gamma(s_j)ds_j \quad (3.3)$$

Resolving dq_{ij} parallel to the surface element s_i , we obtain the following tangential velocity component

$$dv_{ij} = dU_{ij} \cos \beta_i + dV_{ij} \sin \beta_i \quad (3.4)$$

Integrating over the entire surface and including the effect of the non-singular Fredholm integral equation at the element s_i

$$-0.5\gamma(s_i) + \oint k(s_i, s_j)\gamma(s_j)ds_j + W_\infty(\cos \alpha_\infty \cos \beta_i + \sin \alpha_\infty \sin \beta_i) = 0 \quad (3.5)$$

Here the contour integral yields velocity parallel to the i^{th} element due to all bound vortices around the profile.

In the above equation, the last term is the component of W_∞ resolved parallel to the body surface at i and $k(s_i, s_j)$ is the coupling coefficient given by

$$k(s_i, s_j) = \frac{1}{2\pi} \cdot \frac{(y_i - y_j) \cos \beta_i - (x_i - x_j) \sin \beta_i}{(x_i - x_j)^2 + (y_i - y_j)^2} \quad (3.6)$$

For convenience we may write a modified coupling coefficient $K(s_i, s_j)$ by absorbing $0.5\gamma(s_i)$ into it. Thus, i.e.

$$K(s_i, s_j) = k(s_i, s_j)ds_j - 0.50\delta_{ij}ds_i \quad (3.7)$$

Hence equation (3.5) may be written in the numerical form as

$$\sum_{j=1}^M K(s_i, s_j) \gamma(s_j) = -(U_\infty \cos \beta_i + V_\infty \sin \beta_i) \quad (3.8)$$

This is the basic equation of Martensen procedure. These are the details of the numerical strategies adopted here.

3.2.1 Surface element geometry

A set of $(M+1)$ input data coordinates (x_n, y_n) are specified as shown in Fig. 3.2. moving clockwise around the profile from the leading edge. Point $M + 1$ coincides with point 1, ensuring profile closure. Straight panels are obtained by joining successive data points. Elements lengths are then given by

$$\Delta s_n = \sqrt{(x_{n+1} - x_n)^2 + (y_{n+1} - y_n)^2} \quad (3.9)$$

Profile slopes and pivotal points which are located at the center of each element, are then given by

$$\cos \beta_n = (x_{n+1} - x_n) / \Delta s_j \quad (3.10)$$

$$\sin \beta_n = (y_{n+1} - y_n) / \Delta s_j \quad (3.11)$$

$$x_n = \frac{1}{2}(x_{n+1} + x_n) \quad (3.12)$$

$$y_n = \frac{1}{2}(y_{n+1} + y_n) \quad (3.13)$$

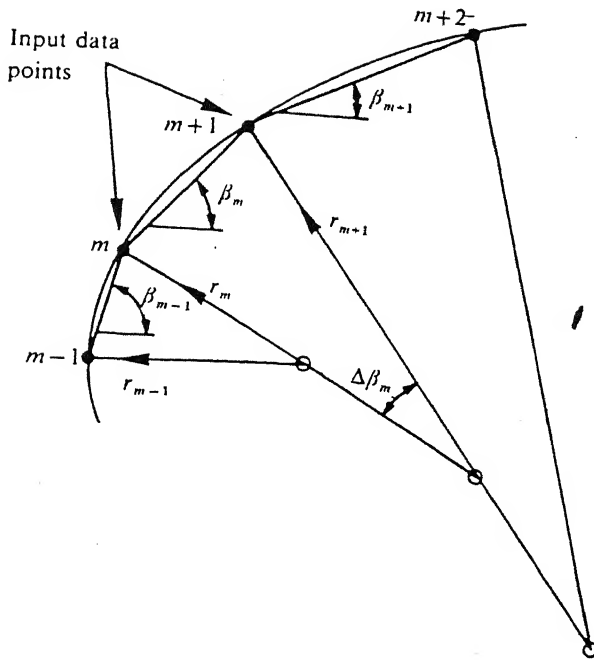


Fig3.2 Surface element geometry

3.2.2 Determination of Coupling coefficients

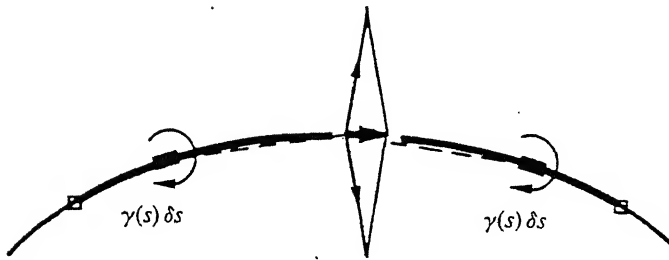
By definition, coupling coefficients $\mathbf{K}(s_i, s_j)$ represents the velocity at s_i parallel to the body surface induced by a unit vortex located at the j^{th} panel. The determination is rather straight forward except for some complications as before.

Effect of Curvature

A curved panel has non-zero value of the self-induced velocity as shown in Fig. 3.3. But the discretization scheme adopted uses straight panels which necessarily have zero self-induction. For better accuracy, the coupling coefficients must be modified so as to take into account the curvature of the body surface. Generally, such calculation involves the use of curve fitting methods, which are not suitable for the cases in which the curvature varies enormously and rapidly in certain locations

of the body profiles. Lewis gives a simple and alternate relation which has been used in the programs here, as

$$K(s_i, s_j) = 0.5 - \frac{(\beta_{i+1} - \beta_{i-1})}{8\pi} \quad (3.14)$$



(b) Finite self-induced parallel velocity of a curved vorticity element

Fig. 3.3. Self-induced velocity of a surface vorticity element.

Use of sub-elements

When the body is thin, the elements opposite a given collocation point come so close that the concentration of the distributed vorticity at the middle point may result in overestimating the influence of that element. This result is manifested mathematically, by the growth of the back diagonal terms in the matrix of coupling coefficient to the order of the diagonal elements (approx 0.5). The easiest way to overcome this is to breakup such elements into a number of sub-elements and to replace the relevant coefficient by the average of the coupling coefficients of the sub-elements.

Consider a case in which a element s_j is broken up into N subelements each of length ds_j/N . The coupling coefficient of this the i^{th} element then is given by

$$K(s_i, s_j) = \frac{1}{\Delta s_j} \int_0^{\Delta s_j} K(s_i, s_j) ds_j \quad (3.15)$$

or in the numerical form

$$K(s_i, s_j) = \frac{1}{N} \sum_{k=1}^N \frac{(y_i - y_k) \cos \beta_i - (x_i - x_k) \sin \beta_i}{(x_i - x_k)^2 + (y_i - y_k)^2} \quad (3.16)$$

where

$$x_k = x_j + (k - 0.5(N + 1)) \frac{\Delta s_j \cos \beta_i}{N} \quad (3.17)$$

$$y_k = y_j + (k - 0.5(N + 1)) \frac{\Delta s_j \sin \beta_i}{N} \quad (3.18)$$

It is found that use of two or three subelements gives better results than using more subelements. We shall use only two subelements in all our calculations.

3.3 Martensen analysis in the presence of a cloud of vortices

In a quasi-steady flow the potential flow past a 2-D body of arbitrary shape in the presence of a cloud of line vortices is described by the boundary integral equation

$$\begin{aligned} -0.5\gamma(s_m) + \frac{1}{2\pi} \oint k(s_m, s_n) \gamma(s_n) ds_n + (U_\infty \cos \beta_m + V_\infty \sin \beta_i) \\ + \sum_{j=1}^Z \Delta \Gamma_j (U_{mj} \cos \beta_m + V_{mj} \sin \beta_m) = 0 \end{aligned} \quad (3.19)$$

where unit velocities U_{mj} and V_{mj} are given by

$$U_{mj} = \frac{1}{2\pi} \cdot \frac{(y_m - y_j)}{r_{mj}^2}, \quad V_{mj} = -\frac{1}{2\pi} \cdot \frac{(x_m - x_j)}{r_{mj}^2} \quad (3.20)$$

with

$$r_{mj}^2 = (x_m - x_j)^2 + (y_m - y_j)^2$$

Here the last term represents the contribution to the Dirichlet boundary condition of zero tangential velocity of the Z line vortex elements of strength Γ_j . In the scheme of calculation developed here, the last two term are shifted to the RHS at each

step the matrix of influence coefficients does not change while the RHS changes (due to convection of vortices and introduction of nascent vortices), it is convenient to use the matrix inversion path to solve the equation.

3.4 Vortex shedding from the body surface

In the application of discrete vortex modelling for the separated flow about bluff bodies, the new vortices are shed into flow field at each time step. Just as in the development of boundary layer described in last chapter, the surface vorticity distribution required to satisfy the no-slip condition at the body at any time step is taken as the vorticity created in the time interval, and as the vorticity diffuses into the flow field. And as before, this vorticity diffuses and convects (essentially along the body surface) forms the thin boundary layer and the wake of the body.

As was assigned in the last chapter, if the diffusion of the vorticity is taken to start from the location of the vortex surface, i.e. at the body surface itself, about one-half of the vortices will move into the body interior right at the first step. Chorin suggests using a vortex sheet of twice the strength so that after the first diffusion, we get the correct strength of the vortices.

An alternate approach is the release of vorticity at some offset from the surface. The offset is determined by equating it to the root mean square drift of vortices in a random-walk step, which is $\sqrt{4\nu\Delta t/3}$. In fact, this step is identical in result to the Chorin scheme, except that the diffusive calculation are reduced by a factor of 2.

3.5 Diffusion of vortices

Diffusion of vortices is modelled by a random walk method similar to that used in the last chapter. Here unlike Chorin(1973), Lewis(1981) and Verma(1994), we have used the point vortex diffusion model, walking randomly in the θ direction with flat

probably, and walking randomly in r direction with normal distribution, as shown in the last chapter. The previous researchers have permitted diffusion only along the body surface on the plea that the resulting term in the boundary layer equations are $\frac{\partial^2 \omega}{\partial y^2}$. But if we note that the original term was $\nabla^2 \omega$ from with the x direction was neglected (compared to x convection), it is clear that using the simpler point diffusion model is quite correct with the added advantage of the formulation already available.

3.6 Convection of vortices

Once the vortices are shed from the body surface, they are free to undergo convection under the combined influence of vortex cloud, bound vorticity on the body surface and external flow field.

Let us focus out attention on a single vortex 'm' located in the flow field at the position (x_m, y_m) Fig. 3.2. If there are Z vortices in the cloud, the velocity at m^{th} vortex will be influence by these vortices. If we consider n^{th} vortex in the cloud located at the position (x_n, y_n) , the velocity at m due to the vortex n will be given by Biot-Savart law as

$$U_{mn} = \frac{\Gamma_n}{2\pi} \cdot \frac{(y_m - y_n)}{r_n^2} \quad (3.21)$$

$$V_{mn} = -\frac{\Gamma_n}{2\pi} \cdot \frac{(x_m - x_n)}{r_n^2} \quad (3.22)$$

we can sum up the influence of Z vortices as

$$U_{m,cloud} = \sum_{\substack{n=1 \\ n \neq m}}^{n=Z} \frac{\Gamma_n}{2\pi} \left\{ \frac{y_m - y_n}{r_n^2} \right\} \quad (3.23)$$

$$V_{m,cloud} = - \sum_{\substack{n=1 \\ n \neq m}}^{n=Z} \frac{\Gamma_n}{2\pi} \left\{ \frac{x_m - x_n}{r_n^2} \right\} \quad (3.24)$$

If there are M discrete panels on the body surface with distributed vorticity of the strength $\gamma(s_n)ds_n$ at the n^{th} element, the combined influence of these bound vortices on the m^{th} free vortex in the wake will be given by

$$U_{m,bound} = \sum_{j=1}^M \frac{\gamma(s_j)ds_j}{2\pi} \left\{ \frac{y_m - y_j}{r_{mj}^2} \right\} \quad (3.25)$$

$$V_{m,bound} = - \sum_{j=1}^M \frac{\gamma(s_j)ds_j}{2\pi} \left\{ \frac{x_m - x_j}{r_{mj}^2} \right\} \quad (3.26)$$

The velocity far upstream the body influence the velocities of the free vortices as

$$U_{m,external} = U_{\infty} \quad (3.27)$$

$$V_{m,external} = V_{\infty} \quad (3.28)$$

The resultant velocity of the m^{th} vortex is simply given by the combined influence of all three terms. Thus we can write

$$u_m = U_{m,external} + U_{m,cloud} + U_{m,bound} \quad (3.29)$$

$$v_m = V_{m,external} + V_{m,cloud} + V_{m,bound} \quad (3.30)$$

Now, for applying the vortex convection, Let us consider a vortices at the position of a and then by using forward difference approach, the revised locations of the free vortices during the time interval is given by

$$x_{mb} = x_{ma} + u_m \Delta t \quad (3.31)$$

$$y_{mb} = y_{ma} + v_m \Delta t \quad (3.32)$$

After convecting all vortices, if we now recalculate the new convection velocities at locations b , (u_{mb}, v_{mb}) , we may march forward again through next time step to the final position. For better estimation of vortex convection, the central difference technique in which the effect of the curvature of the drift path is also considerable is used like that,

$$x_{m,final} = x_{ma} + 0.5(u_{ma} + u_{mb})\Delta t \quad (3.33)$$

$$y_{m,final} = y_{ma} + 0.5(v_{ma} + v_{mb})\Delta t \quad (3.34)$$

3.6.1 Convection of vortices in very close proximity to body surface

In the last section, we had mentioned some difficulties while calculating the coupling coefficient by the use of Biot-Savart law alone. Such problems are again encountered when calculating the velocities of vortices which have drifted too close to the body surface. It is observed that even the use of sub-elements does not yield good results when the gap ratio $\epsilon/\Delta s$ is less than 0.40. In such cases we go for the 'Mirror Image Technique' to calculate the velocities.

Mirror image technique

If the gap ratio $\epsilon/\Delta s$ is less than 0.40, then the velocity of the vortex is calculated by the use of simple mirror image technique. If we assume that the panels are straight, then the convective velocity of the vortex is given by

$$q_d = -\frac{\Delta\Gamma_n}{4\pi\epsilon} \quad (3.35)$$

where q_d is parallel to the panel. While using this formula we neglect the U_∞ and V_∞ components of the velocities.

We shall summarise the techniques available to us for the calculation of velocities of free vortices

(1) For gap ratios, $\epsilon/\Delta s > 1.0$ normal surface vorticity modelling will suffice without the use of sub-elements.

(2) For $1.0 > \epsilon/\Delta s > 0.4$ sub-elements should be used when calculating the convective velocity due to the bound vorticity.

(3) For $\epsilon/\Delta s < 0.40$ mirror image modelling should be used.

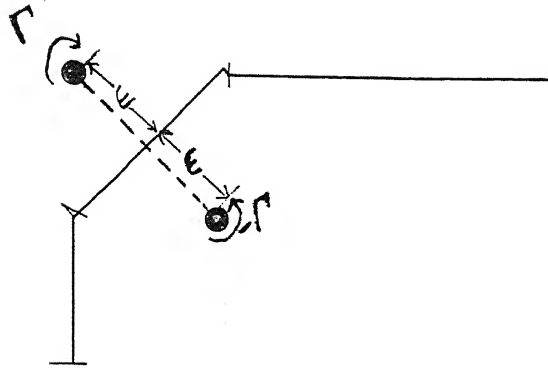


Fig 3.4. Mirror Image system for self-induced convection

Some other difficulties that arise when simulating flow behind bluff bodies using vortex element techniques are

1 Vortices may accidentally stray inside body contour due to inaccurate convection routines.

2 Vortices may drift too close to the body (so that even mirror image technique fails to calculate the actual velocity). These vortices may generate serious potential flow errors or excessive self-convection velocities.

Selection of element size and time step

An appropriate device of the time step Δt is one in which the convective and diffusive displacement are of the order of the element size. Thus, the convective displacement δ_c which is of order $\frac{1}{2}U\Delta t_c$ should be of the same order as the element size, say $\frac{l}{2M}$, M being the number of panels taken along the body. This gives the convective time step as $\Delta t_c \approx \frac{l}{MU}$.

The typically diffusive displacement on the other hand is

$$\Delta r_i = [4\nu \Delta t \ln(\frac{1}{P_i})]^{1/2} \quad (3.36)$$

got from Equation 2.25. by as $\delta_d \approx [4\nu \Delta t \ln 2]^{1/2}$, so that

$$\delta_d \approx [4\nu l \ln 2 / MU]^{1/2} \quad (3.37)$$

or

$$\frac{\delta_d}{\frac{l}{2M}} \approx M^{\frac{1}{2}} \left(\frac{4\nu}{Ul} \right)^{\frac{1}{2}} \quad (3.38)$$

$$= \left(\frac{16M}{\text{Re}} \right)^{\frac{1}{2}} \quad (3.39)$$

or

$$\Delta t = \frac{16l \ln 2}{U \text{Re}} \quad (3.40)$$

For very large Reynolds numbers then, we see that the diffuse displacement time step is extremely small. A considerable saving in calculation effort can be effected by choosing different time scales for diffusion and convection.

Thus, with reference to Equation 2.14, we choose $\Delta t = \Delta t_D$ such that $\delta_D \approx \frac{l}{2M}$, so that

$$\Delta t_D = \frac{l^2}{16\nu M^2 \ln 2} \quad (3.41)$$

The ratio of the diffusive time step Δt_D to the convective Δt_c then is

$$\frac{\Delta t_D}{\Delta t_c} = N_t = \frac{\text{Re}}{16M \ln 2} \quad (3.42)$$

3.7 Zero circulation condition for RHS term

The necessary condition that the net circulation around the cylinder perimeter due to the externally located vortex Γ must be zero, requires that, all the vortices in the wake behind a body should produce net zero circulation on the body surface. If this

condition were not satisfied, there will be an implied erroneous residual vorticity bound within the body profile leading to a flux through the body surface for this shown a zero circulation condition is built into the RHS. The influence of the vortex cloud on the m^{th} element on the body surface makes that following contribution to the RHS

$$RHS_{m,cloud} = \sum_{j=1}^Z \Delta\Gamma_j (U_{mj} \cos \beta_m + V_{mj} \sin \beta_m) \quad (3.43)$$

Circulation around the whole body surface can then be written as

$$\sum_{n=1}^M RHS_{n,cloud} \Delta s_n = 0.0 \quad (3.44)$$

To ensure this, then, at each step the largest value of $RHS_{p,cloud}$ is replace by

$$RHS_{p,cloud} = -\frac{1}{\Delta s_p} \sum_{\substack{n=1 \\ n/neqp}}^M RHS_{p,cloud} \Delta s_n \quad (3.45)$$

3.7.1 Conservation of vortices

In accordance with Helmholtz theorem the vorticity should be conserved at all times and hence if the vorticity is zero everywhere when the flow starts, it should be zero all through. We can write this in terms of mathematical formula

$$\sum_{n=1}^M \gamma(s_n) ds_n + \sum_{j=1}^Z \Delta\Gamma_j - \Gamma_{circ} = 0 \quad (3.46)$$

where Γ_{circ} is the cumulative strength of all the vortices which are snuffed out for various reasons as the calculations proceeds. This equation must be added to each of the governing equations to ensure that vorticity is continually being conserved.

Thus, we can write the most general equation as follows.

$$\begin{aligned} \sum_{n=1}^M (k(s_m, s_n) + \Delta s_n) \gamma(s_n) = & -W_{\infty} \cdot \cos(\alpha_{\infty} - \beta_m) \\ & + \Gamma_{circ} - \sum_{j=1}^Z \Delta\Gamma_j \cdot (1 + U_{mj} \cos \beta_m + V_{mj} \sin \beta_m) \end{aligned} \quad (3.47)$$

3.8 Merge and Reflection of the Vortices

As we are releasing M vortices at every time step the number of vortices in the flow field will grow unless some action is taken. There is a need to curb the rise in number of vortices in the flow field because of the following reasons

1. The CPU time is directly proportional to the N^2 , where N is the number of vortices in the flow field.
 2. As the vortices come closer, they will induce excessive velocities on each other.
 3. The influence of the vortices on the body surface decreases with the distance.
- Therefore computational efforts can be minimized if we can reduce the number of vortices in the flow field.

For these reasons, we shall merge those vortices which have come too close to each other than some specified distance. The merging is done using exactly the same manner as done in the previous chapter for calculating the boundary layer on a flat plate.

3.9 Calculation of surface pressure distribution and forces

Once convection and diffusion have been completed in the numerical simulation The Navier-Stokes equations reduces to

$$\frac{\partial \mathbf{q}}{\partial t} = -\frac{1}{\rho} \nabla p_s \quad (3.48)$$

At any point s_n on the body surface, the velocity \mathbf{q} parallel to the surface is given by $\gamma(s_n)$. Therefore,

$$\frac{\partial p_s}{\partial s} = -\rho \frac{\partial \gamma(s_n)}{\partial t} \quad (3.49)$$

from which we can directly calculate the numerical for the change in surface pressure over the surface element n during the time step Δt value of

$$\Delta p_n = -\rho \frac{\gamma(s_n) \Delta s_n}{\Delta t} = -\rho \frac{\Gamma_n}{\Delta t} \quad (3.50)$$

Equation may be integrated to yield the surface pressure at any point on the body

$$p_m = p_{stag} - \frac{\rho}{\Delta t} \sum_{j+1}^M \Gamma_j \quad (3.51)$$

Average lift and coefficients can be calculated from the values of pressures.

Spectral analysis technique is used for finding out the dominant frequencies f of the excitation forces. From this dimensionless frequency can be expressed from the Strouhal number

$$St = \frac{fd}{W_\infty} \quad (3.52)$$

3.10 Determination of Lift and Drag coefficient

Once the static pressure distribution is known around the body surface, lift and drag coefficient can be estimated from the following equations

$$C_L = \frac{L}{0.5\rho W_\infty^2 l} = -\frac{2}{\rho W_\infty^2} \sum_{n=1}^M \bar{p}_n \cos \beta_n \Delta s_n \quad (3.53)$$

$$C_D = \frac{D}{0.5\rho W_\infty^2 l} = \frac{2}{\rho W_\infty^2} \sum_{n=1}^M \bar{p}_n \sin \beta_n \Delta s_n \quad (3.54)$$

where l is the characteristic length and $\bar{p}_n = 0.5(p_n + p_{n+1})$ is the average pressure on element n

3.11 Results and discussions

For the application of full vortex cloud analysis we have considered two geometries, a circular cylinder and a square cylinder. We have studied the flow past these bodies at various Reynolds number. In these applications, we first divided the body surface into a number panel. Vortices of appropriate strengths are shed from each elements normal to the surface at each time steps. These newly created vortices are subjected to diffuse by the random walk technique as discussed earlier in detail. After that we merge the two vortices into one vortex when the distance between these two vortices is less than the specified distance and vortices which drifted under the body surface are reflected back to that position at each iteration. The time step is taken around 0.12 as per rule and the case was run for 250 time steps ($T_{max} = 30.0$) which is sufficiently large to cover several oscillations of the vortex sheet. Finally, the drag and lift coefficients has been calculated for both the bodies at various Reynolds number (20000, 30000, 40000 and 50000) and then, strouhal number has been also calculated by using the technique of spectral analysis.

Flow past the circular cylinder

For the case of circular cylinder in which the main stream flow U_{∞} is 1.0, we take the diameter of the circular cylinder 1.0 and discretize the body into the 32 surface element. For eliminating the numerical noise, we are averaging over two time steps in the calculation of lift and drag coefficients. The flow diagram for different Reynolds number are shown in Fig. 3.5. to Fig. 3.8. in which we have considered three different times (6.0, 12.0 and 30.0). where as the variation of the lift and drag coefficients w.r to time is shown from Fig. 3.9. to Fig. 3.13. Table 3.1. shows the average values of the drag and lift coefficients with the Strouhal number. But there was lot of numerical noise in the pressure calculation so that we could get quite

higher values of drag and St.

Table 3.1. For the case of circular cylinder

Re	<i>Average Drag coefficients</i>	<i>Average Lift coefficients</i>	St
20000	3.1144	6.655E-02	0.3448
30000	3.2547	4.384E-02	0.3540
40000	3.2466	1.424E-02	0.3478
50000	2.8849	-1.674E-02	0.3288

Flow past a square cylinder

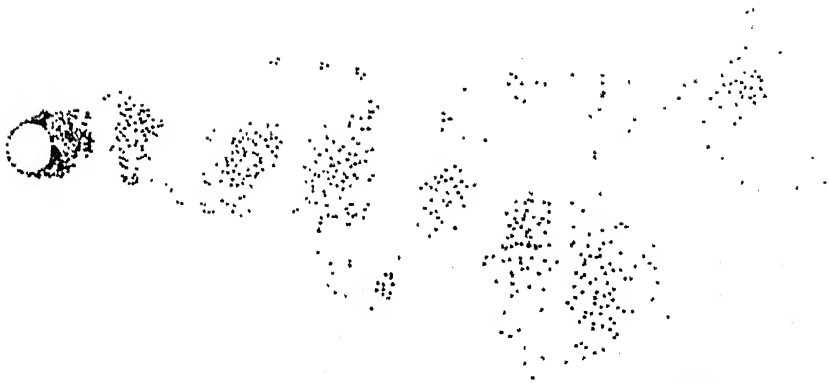
For the case of a square cylinder, main stream flow is same as circular cylinder and the side of the square is also 1.0 we discretize the body into 36 surface element. The flow diagram for different Reynolds number are shown in Fig. 3.14. to Fig. 3.17. as the case of circular cylinder and the variation of the lift and drag coefficients w.r to time are shown from Fig 3.18 to Fig 3.21. Table 3.2 is in same pattern as Table 3.1, for the square cylinder. We get higher values of drag due to the problem of numerical noise in the pressure calculation. This is very difficult problem which we face in this method.

Table 3.2. For the case of square cylinder

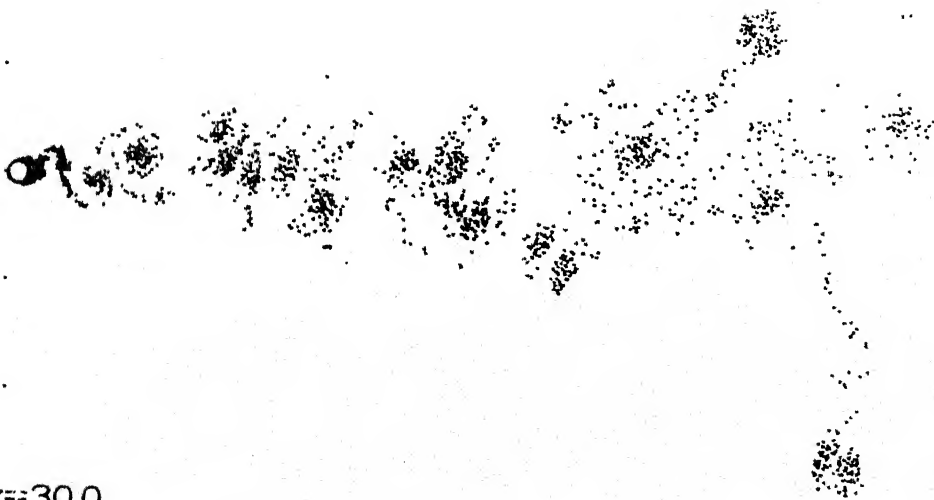
Re	<i>Average Drag coefficients</i>	<i>Average Lift coefficients</i>	St
20000	3.6827	3.324E-02	0.2663
30000	3.6743	4.526E-02	0.2690
40000	3.8223	3.628E-02	0.2681
50000	3.8013	4.228E-02	0.2672



(A) $T_{\max} = 6.0$



(B) $T_{\max} = 12.0$



(C) $T_{\max} = 30.0$

Fig. 3.5. Full vortex cloud solution for circular cylinder at $Re = 20000$

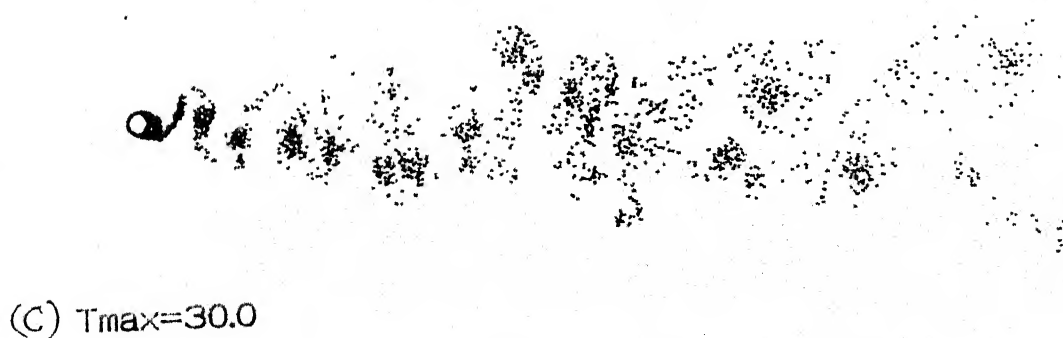


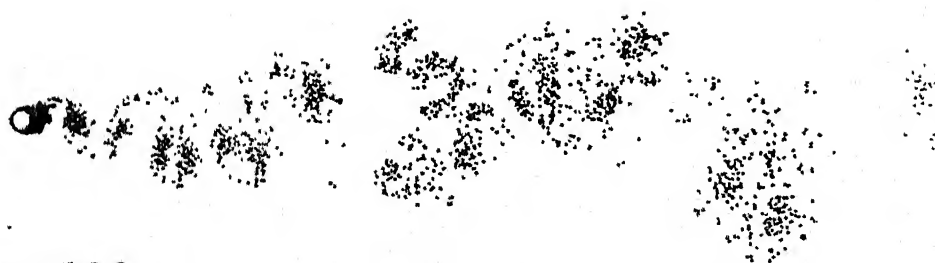
Fig. 3.6. Full vortex cloud solution for circular cylinder at $Re = 30000$



(A) $T_{\max} = 6.0$



(B) $T_{\max} = 12.0$



(C) $T_{\max} = 30.0$

Fig. 3.7. Full vortex cloud solution for circular cylinder at $Re = 40000$



(A) $T_{\max} = 6.0$



(B) $T_{\max} = 12.0$



(C) $T_{\max} = 30.0$

Fig. 3.8. Full vortex cloud solution for circular cylinder at $Re = 50000$

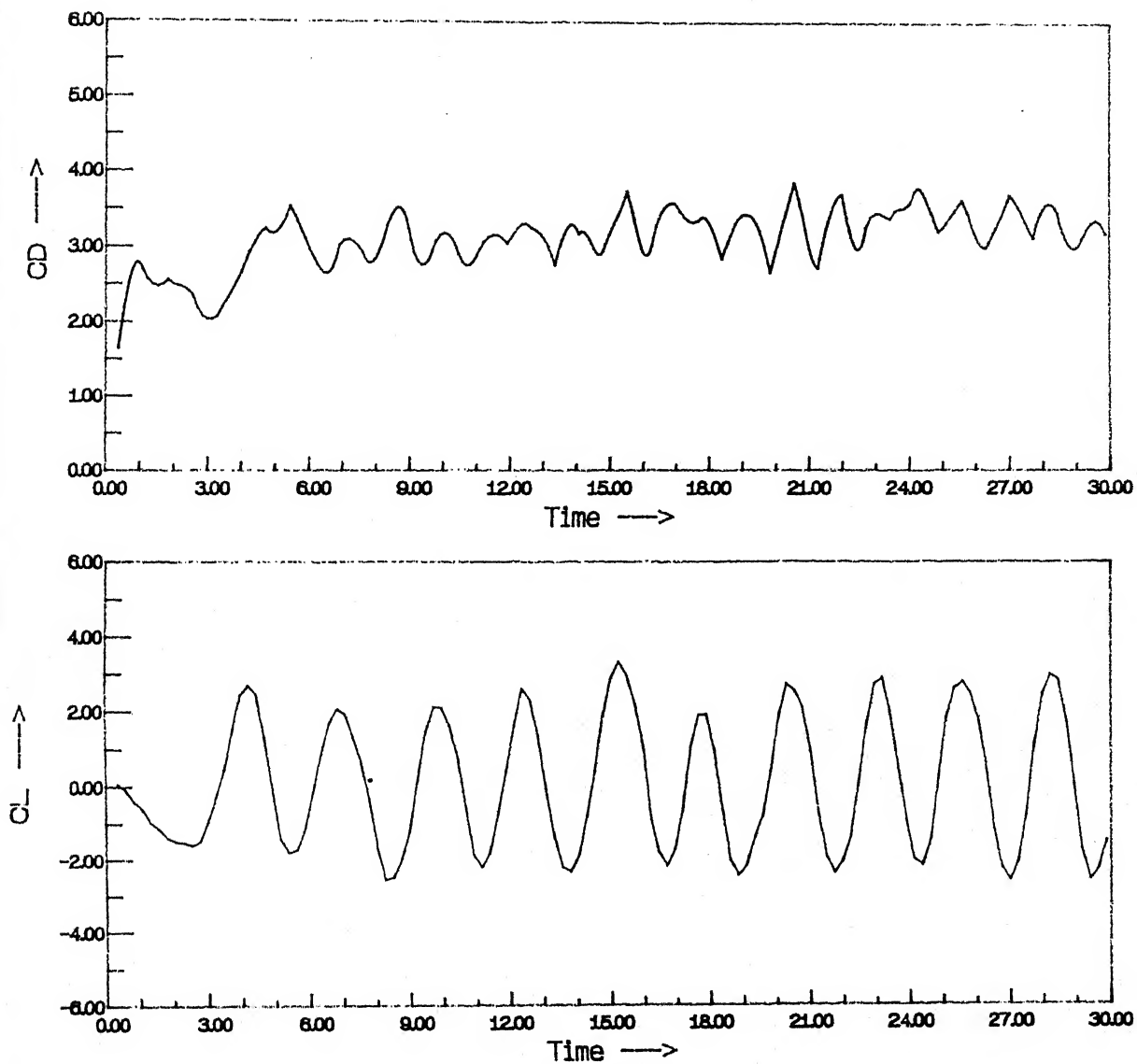


Fig. 3.9. Lift and drag coefficients on a circular cylinder at $Re = 20000$

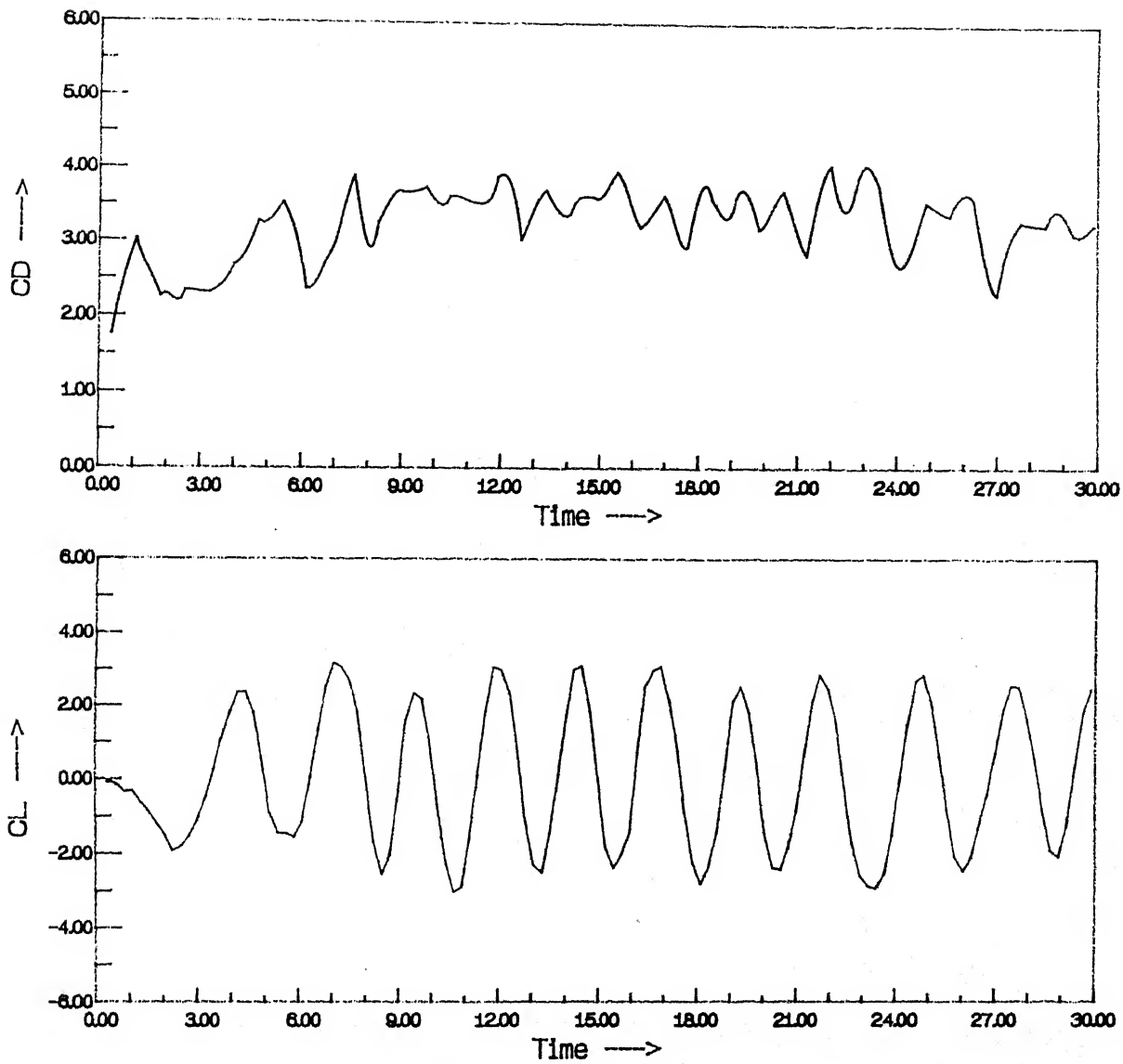


Fig. 3.10. Lift and drag coefficients on a circular cylinder at $Re = 30000$

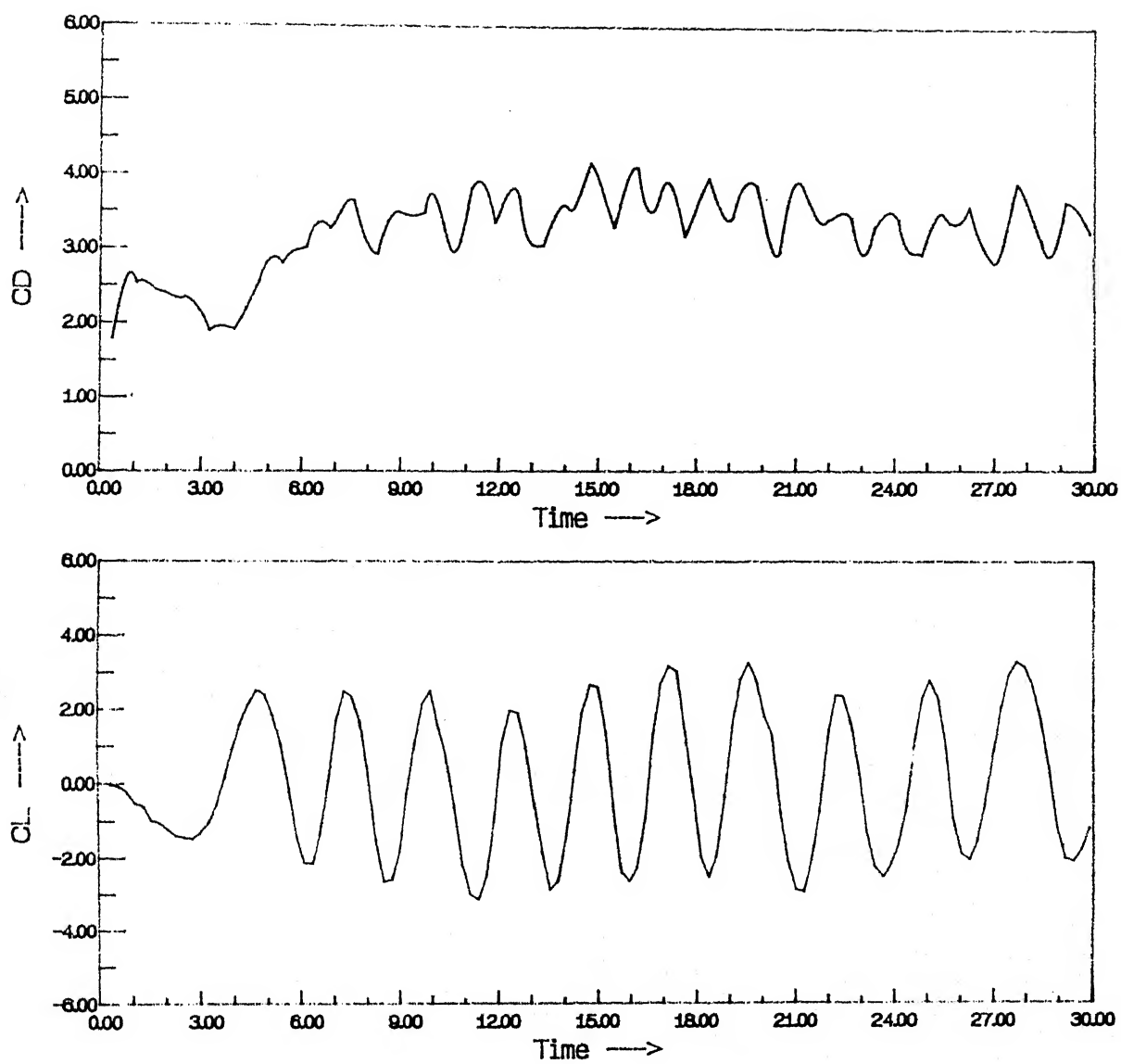


Fig. 3.11. Lift and drag coefficients on a circular cylinder at $Re = 40000$

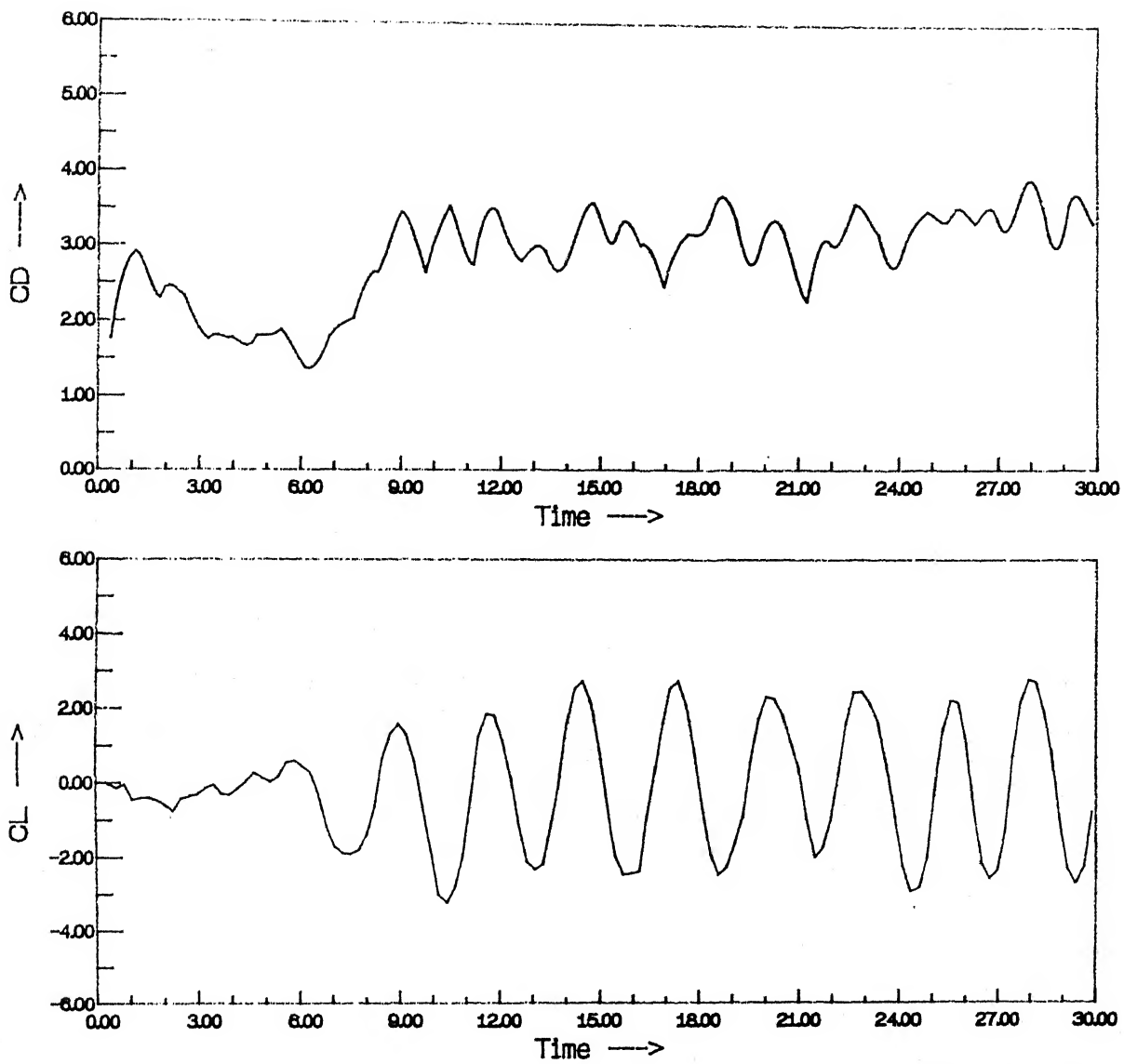


Fig. 3.12. Lift and drag coefficients on a circular cylinder at $Re = 50000$



(A) $T_{max} = 6.0$



(B) $T_{max} = 12.0$



(C) $T_{max} = 30.0$

Fig. 3.13. Full vortex cloud solution for square cross section at $Re = 20000$



(A) $T_{\max}=6.0$



(B) $T_{\max}=12.0$



(C) $T_{\max}=30.0$

Fig. 3.14. Full vortex cloud solution for square cross section at $Re = 30000$



(A) $T_{\max} = 6.0$



(B) $T_{\max} = 12.0$



(C) $T_{\max} = 30.0$

Fig. 3.15. Full vortex cloud solution for square cross section at $Re = 40000$



(A) $T_{max}=6.0$



(B) $T_{max}=12.0$



(C) $T_{max}=30.0$

Fig. 3.16. Full vortex cloud solution for square cross section at $Re = 50000$

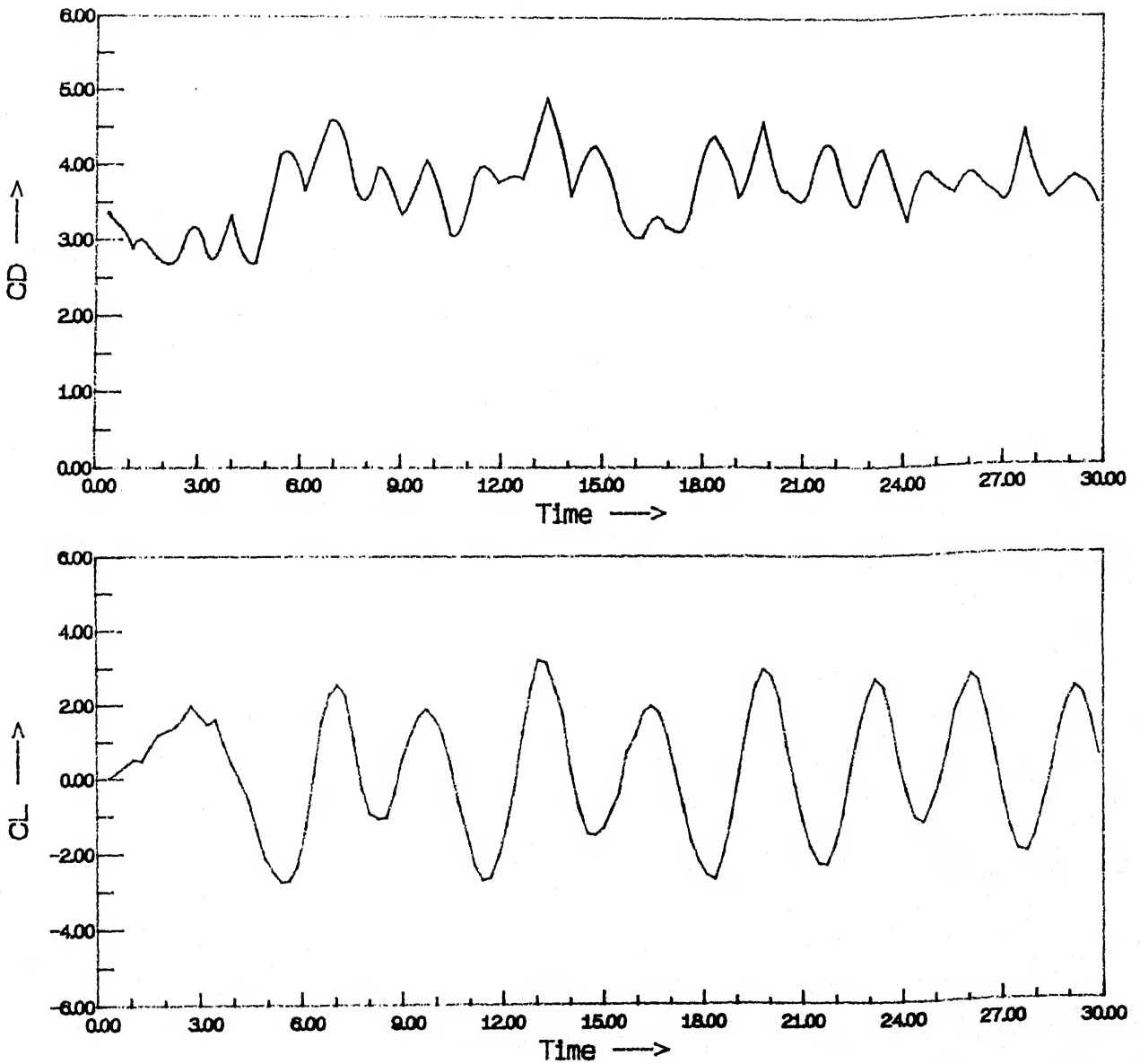


Fig. 3.17. Lift and drag coefficients on a square cross section at $Re = 20000$

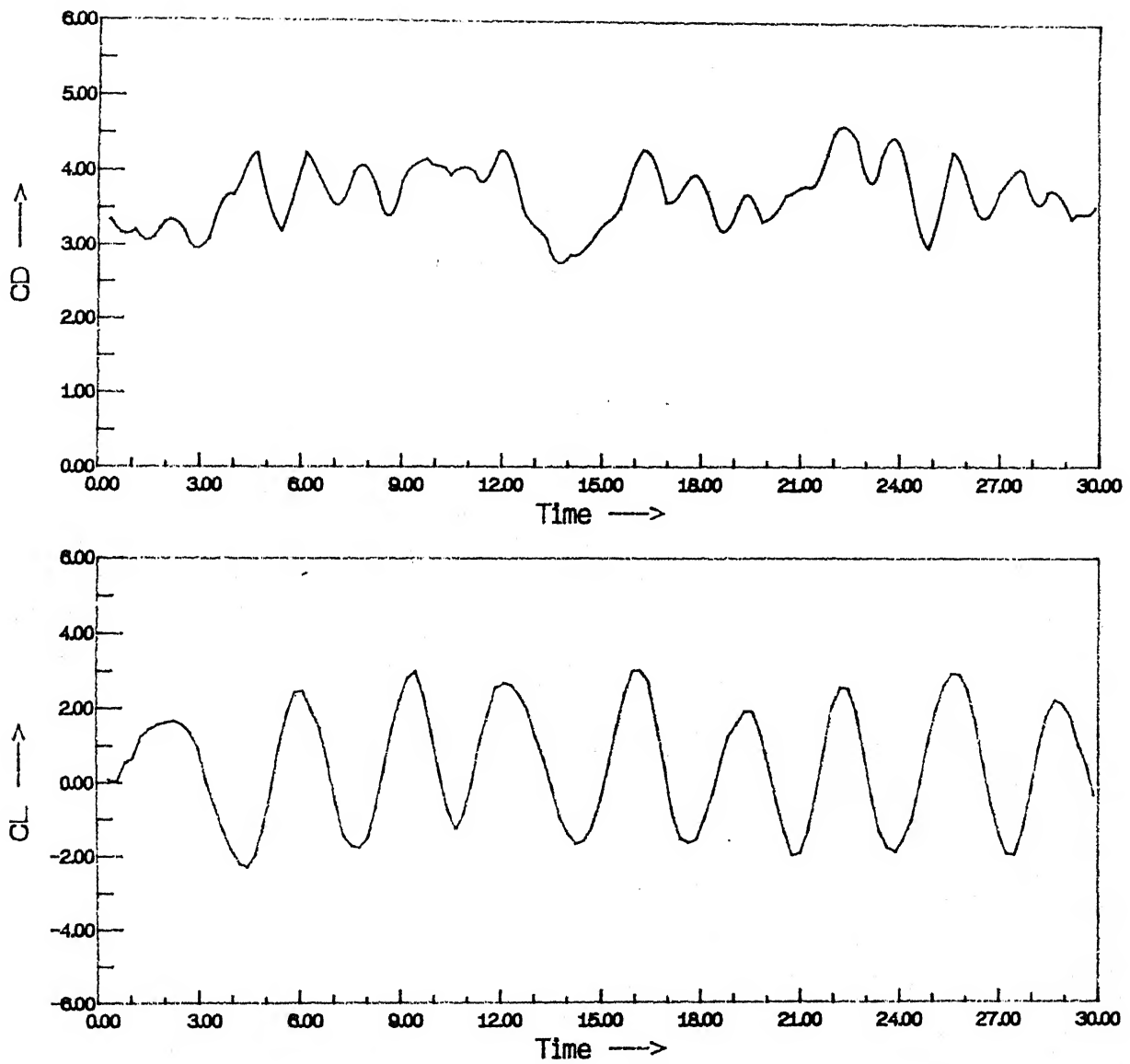


Fig. 3.18. Lift and drag coefficients on a square cross section at $Re = 30000$

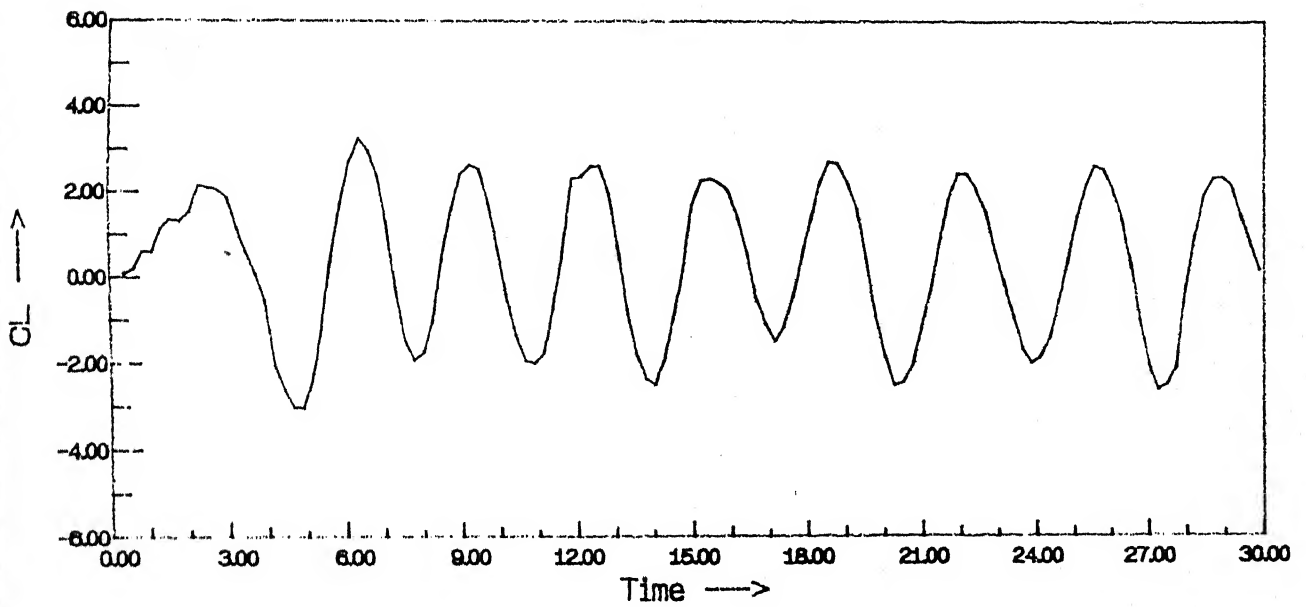
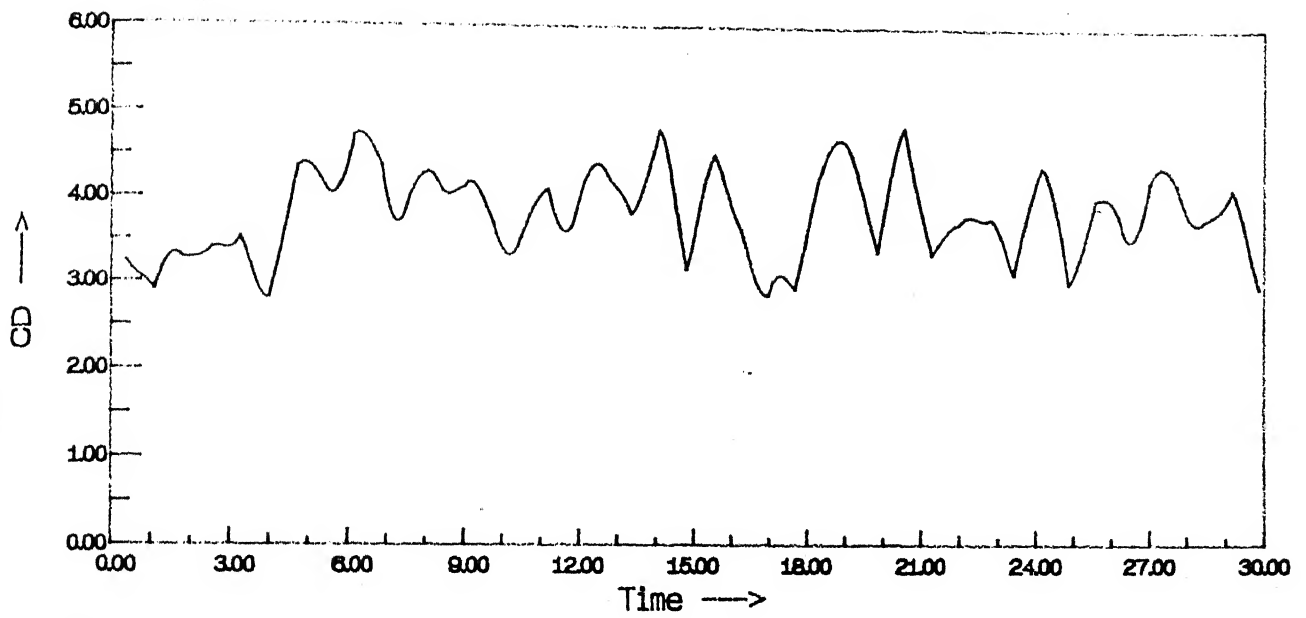


Fig. 3.19. Lift and drag coefficients on a square cross section at $Re = 40000$

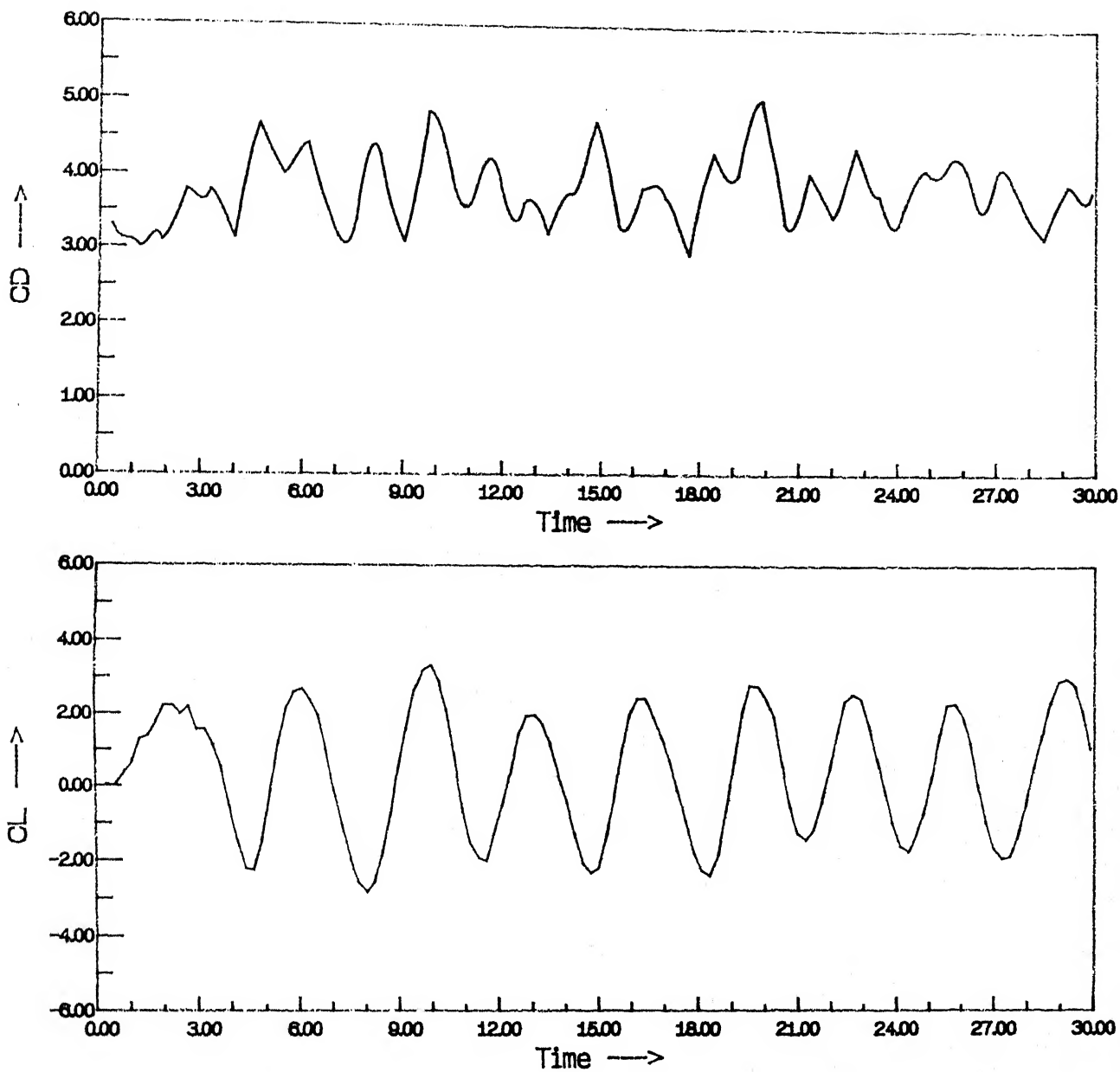


Fig. 3.20. Lift and drag coefficients on a square cross section at $Re = 50000$

Chapter 4

THE FLOW PAST THE MULTIPLE BODIES

4.1 General Introduction

This chapter describes an attempt to simulate the flow past multiple two dimensional bodies by full-vortex cloud method. The procedure closely follows ~~that~~ described in the previous chapter for a single body.

Consider the flow past the P bodies of an arbitrary shape in the (x-y) plane, immersed in a uniform flow W_∞ at an angle of attack α_∞ measured with respect to x-axis. We discretize the surface q_{th} into M_q elements with q taking values from 1 to P , Then, the flow past an assembly of P mutually interacting bodies may be represented by a simple adaptation of equation (3.8) to read

$$\sum_{q=1}^P \sum_{n=1}^{M_q} K_{mn}^{pq}(s_{qn}) = -(U_\infty \cos \beta_{pm} + V_\infty \sin \beta_{pm}) \quad (4.1)$$

where

$$p = 1, 2, \dots, P \text{ and } m = 1, 2, \dots, M_p$$

Equation 4.1 states the Dirichlet boundary condition at surface element i of body p . In the case of multiple bodies the coupling coefficients matrix includes the contributions from all the elements ($n = 1, 2, \dots, M_q$) on each of the bodies ($q = 1, 2, \dots, P$). The number of elements M_q chosen for each body may differ depending upon the individual geometrical requirements.

The coupling coefficient representing the induced velocity at the pivotal point m of body p due to element n of body q is then given by

$$K_{mn}^{pq} = \frac{\Delta s_{qn}}{2\pi} \left\{ \frac{(y_{pm} - y_{qn}) \cos \beta_{pm} - (x_{pm} - x_{qn}) \sin \beta_{pm}}{(x_{pm} - x_{qn})^2 + (y_{pm} - y_{qn})^2} \right\} \quad (4.2)$$

For this case the self-inducing coupling coefficient when ($p = q$ and $m = n$) are given as before single body in equation 2.12.

$$K_{mm}^{pp} = 0.5 - \frac{\beta_{p(m+1)} - \beta_{p(m-1)}}{8\pi} \quad (4.3)$$

The present investigation was started with a shape of finiting, the relative reduction of drag by the various edge treatments that are being proposed for reducing drag of trucks and like shaped vehicles. The geometry for this example is a preliminary shape chosen to develop confidence in the method developed. We choose a square in a close proximity of a rectangle as shown in Fig. 4.1. Then, the general equation to solve the potential flow can be expressed in matrix form as follows where the right hand side remains same as discussed earlier.

$$\begin{pmatrix} A_{11} & A_{12} \\ A_{21} & A_{22} \end{pmatrix} (\gamma(s)) = (rhs) \quad (4.4)$$

where the coupling coefficient matrix has been partitioned to clarify the various body interaction. Thus typically, the sub-matrix A_{12} contain all of the coefficients accounting for the interference experienced by first body due to the second body. The submatrix forming the main diagonal A_{11}, A_{22} etc, account for the influence of each body upon itself and are thus identical to those obtained for each body

considered in isolation. It may be noticed that there are a large number of cross-influence terms signifying that the interactive effect is critical.

The most critical aspect of formulation was the treatment of the terms involve panels which are in close proximity but happen to be on diffused bodies, and in keeping track of zero circular condition, and in effecting internal circular correction.

4.2 Modification for bodies in close proximity

When the bodies are very close to each other, there is the certainty of numerical errors should the gap between point pm and qn on adjacent bodies be less than the local element lengths Δs_{pm} or Δs_{qn} , In that kind of case modification is needed to the i_{th} coupling coefficients in column n by the value

$$K_{in}^{pq} = -\frac{1}{\Delta s_{pi}} \sum_{\substack{m=1 \\ m \neq i}}^{M_q} K_{mn}^{pq} \Delta s_{pm} \quad (4.5)$$

The k_{th} element of body p should be the one in close proximity to element n of body q , as shown in Fig. 4.1.

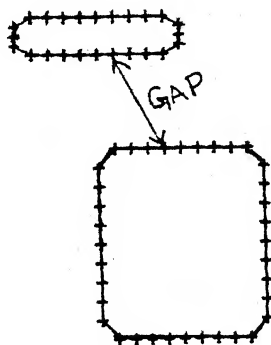


Fig. 4.1. Flow past a square in close proximity of a rectangle.

4.3 Results and discussions

For the application of flow past the multiple two dimensional bodies, we have considered two geometries (a square cylinder and a rectangle cylinder) and, then studied at various Reynolds number (20000, 30000, 40000 and 50000).

The body of the square cylinder and the rectangle cylinder were discretized into 36 surface elements and 22 elements. The side of the square cylinder was taken 1.0 and the sides of the rectangle cylinder were taken 1.0 and 0.2. Thus, 60 vortices of appropriate strengths are shedded from the bodies surfaces at each time step, and, then diffusion and convection were as usual.

The flow diagrams are shown in Fig. 4.2 to Fig. 4.5. for the time 30.0. at each Reynolds number. There are two figures shown in each Fig. in which both figures are similar but second one is the in large version of first.

The main problem in this method we faced that, there are lot of fluctuations in the calculation of pressure distribution due to the numerical noise. We tried a lot to get better results for pressure distribution but due to the numerical noise we could not get. The fairly large time step was a reduction in numerical noise. But by this idea, we have developed a general procedure by which we can obtain the flow diagram of any two dimensional multiple bodies, in which the CPU time is very less.

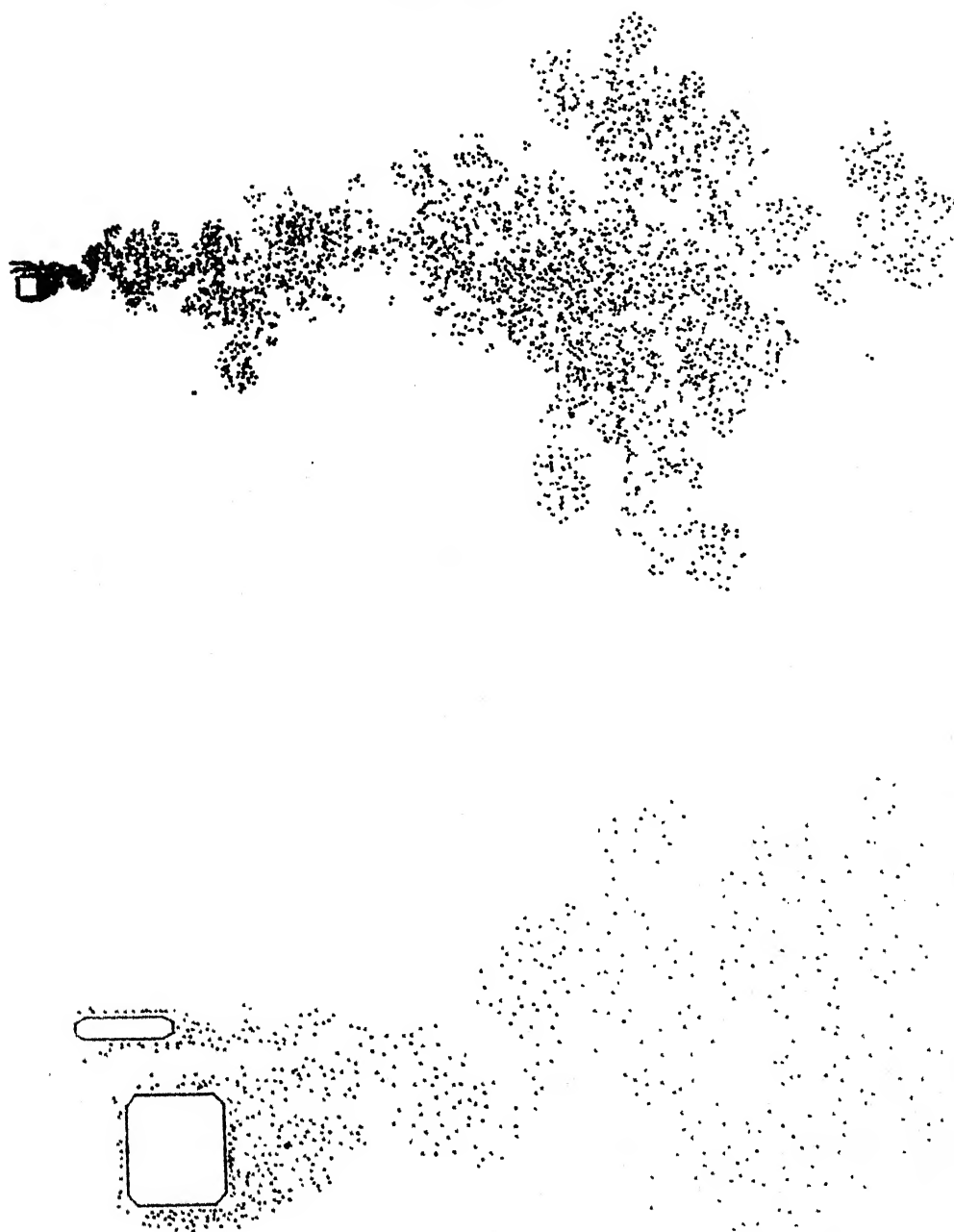
$T_{\max}=30$ 

Fig. 4.2. Full vortex cloud solution for two multiple bodies at $Re = 20000$

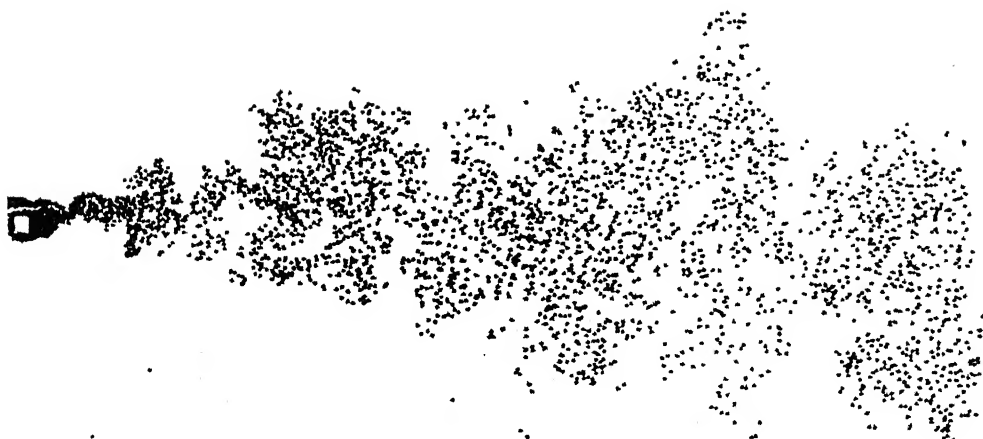
$T_{\max}=30$ 

Fig. 4.3. Full vortex cloud solution for two multiple bodies at $Re = 30000$

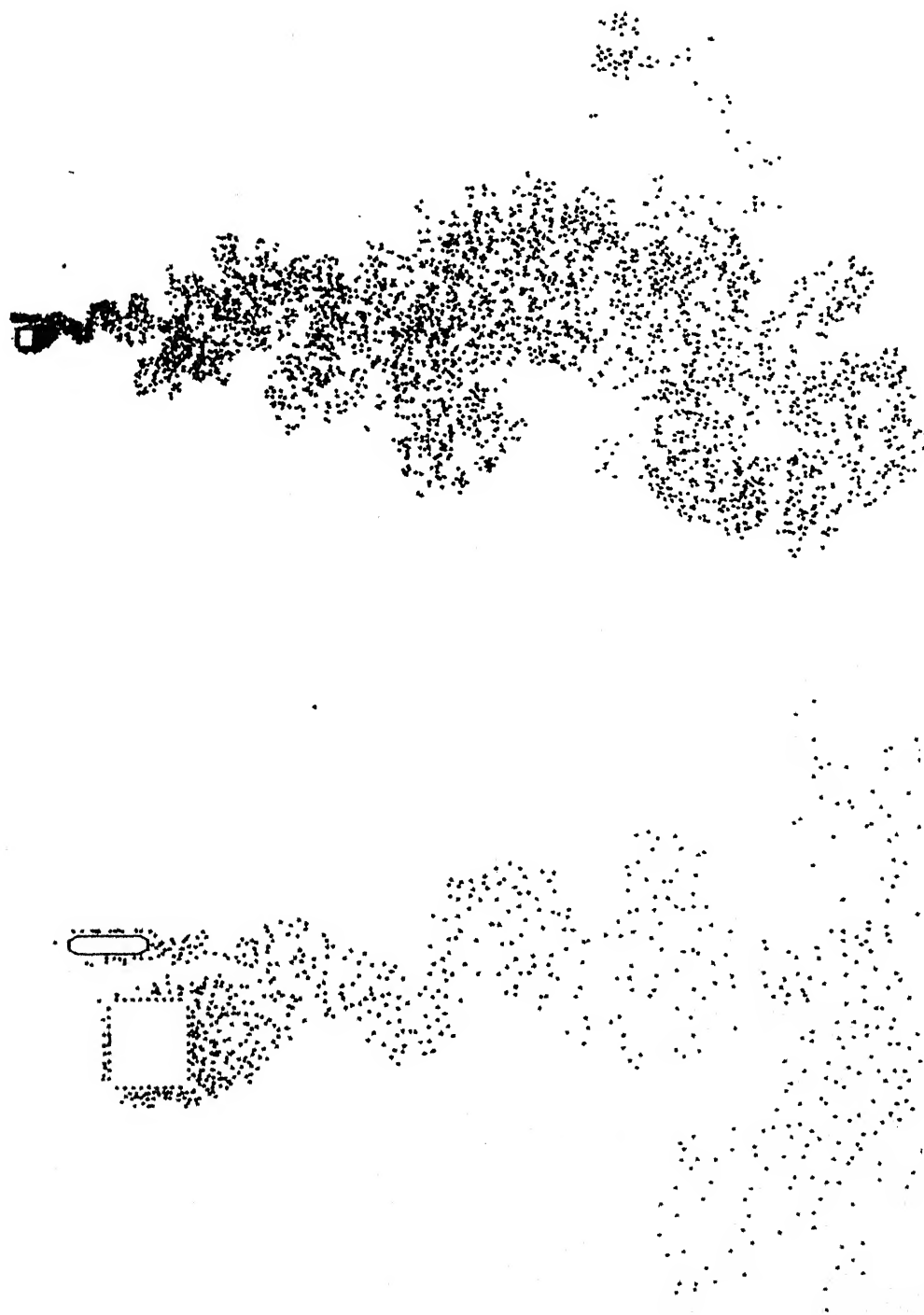
$T_{\max}=30$ 

Fig. 4.4. Full vortex cloud solution for two multiple bodies at $Re = 40000$

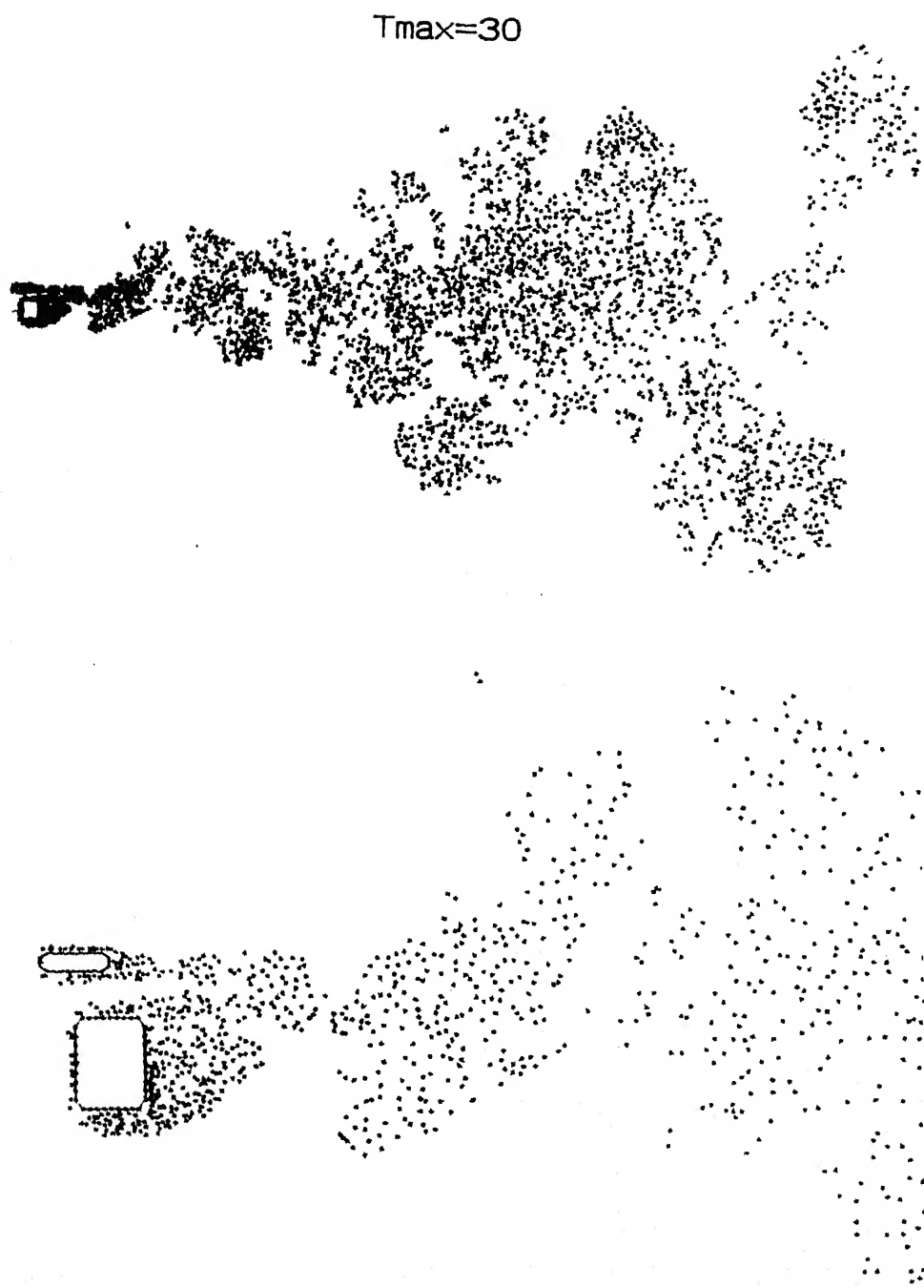


Fig. 4.5. Full vortex cloud solution for two multiple bodies at $Re = 50000$

Chapter 5

CONCLUSIONS

In the first part of the present work, we developed a procedure for the simulation of viscous diffusion in a boundary-layer flow. An operator splitting algorithm has been developed in which the viscous diffusion and convection are treated one after the other. The random walk technique is used for simulation of viscous diffusion. The boundary-layer velocity profile is calculated at one station and compared with theoretically obtained profile. At these values of moderate Reynolds numbers (500, 1000 and 2000), the computed velocity profile is in fairly good agreement with the Blasius profile. The velocity profile has also been calculated at large Reynolds numbers (50000, 100000), for boundary-layer on a flat plate. It was observed that the velocity profile obtained is typical of the turbulent boundary-layer, and there appears to be a fair agreement with the law of the wall.

The second part of the thesis is the simulation of the flow past a bluff body using the full-vortex cloud modelling by the surface vorticity boundary integral method. It develops a discrete vortex element model wherein the body is represented by a number of discrete vortex panels, and vortices in the wake are discretized into individual vortices being shed periodically. The strengths of the vortices are related directly to the tangential velocity outside the boundary-layer. The tangential

boundary condition is satisfied at a number of collocation points through an integral equation. The full-vortex cloud model handles both diffusion and convection of vortices from the surface of the body. The convection of all discrete vortices takes place under the influence of all other discrete vortices and uniform stream velocity, whereas the viscous diffusion of all shed discrete vortices is simulated by using random walk technique. In this model vortices are continuously shed from the surface of the body into the flow fields and are free to move under the combined influence of vortex cloud and the external flow field. Finally the drag and lift coefficients are calculated by getting pressure distribution on the surface of the body and compared with the available data. We get good representation of the nature of the wake but the pressure calculation suffer from too much numerical noise.

In the last part of this thesis an attempt is made to develop a procedure for calculating the flow past multiple two-dimensional bodies. We assembled two mutually interacting bodies and calculated the combined effect after carefully considering the mutual interaction. We got the satisfactory vortex cloud solution for various Reynolds numbers. The pressure distribution and force coefficients are not satisfactory

It appears that this formulation has the following advantages:

- (1) The CPU times involve are an order of magnitude long if we adopt any other method of simulation of viscous flow.
- (2) Change in shapes and conditions are relatively easily handled in this procedure so that quick calculation are possible with changed geometries.

The main disadvantage in the method lies in the fact that calculation of pressure is still not fully understood. There is a lot of numerical noise in pressure calculation in unsteady flow, and the results are not yet satisfactory.

BIBLIOGRAPHY

1. Abernathy F.H. and Kronauer R.E. (1962) The formation of vortex streets. *J. Fluid Mechanics*. 13, 1-20
2. Baker, G.R. (1979) The 'cloud in cell' technique applied to the roll up of vortex sheets. *J.Compu. Phys.*,31, 76-95.
3. Batchelor G.K. (1970) An introduction to fluid dynamics. *Cambridge University Press* .
4. Chaman Singh Verma (1994) Flow about bluff bodies by surface vorticity method. *M.Tech. Thesis, Indian Institute Of Technology, Kanpur*
5. Chorin A.J. (1973) Numerical study of slightly viscous flow. *J.Fluid Mechanics*, 57, 785-796
6. Chorin A.J. (1978) Vortex sheet approximation of Boundary Layers. *J. Computational Physics*, 27, 428-442
7. Clements R.R. (1973) An inviscid model of 2-D vortex shedding. *J.Fluid Mechanics*, 57, 321 .
8. Clements R.R. and Maull, D.J.(1975) The representation of sheets of vorticity by discrete vortices. *Prog. Aero. Sci.*, 16(2), 129-146. .
9. Kiya M. and Arie, M. (1977) A contribution to an inviscid vortex shedding for an inclined flat plate in uniform flow. *J.Fluid Mechanics*, 82, 223-240 .
10. Kiya M. and Arie, M. (1980) Discrete vortex simulation of unsteady separated flow behind a nearly normal plate. *Bulletin of JSME*, 23, No. 183, 1451-1458.
11. Kuwahara K. (1973) Numerical study of flow past an inclined flat plate by an inviscid model. *J.Phys. Soc. Japan*, 35, No.5, 1545-51.

12. Leonard A. (1980) Vortex methods for the flow simulation. *J.Computational Physics*, 37, 289-335.
13. Lewis R.I. (1991) Vortex element methods for fluid dynamic analysis of engineering systems . *Cambridge University Press* .
14. Lewis R.I. (1981) Surface vorticity modelling of separated flows from two-dimensional bluff bodies of arbitrary shape. *Journal of Mechanical Engineering science*, 23, 1-12.
15. Mair W.A. and Maull D.J. (1971) Bluff bodies and vortex shedding -A report on Euromech 17. *J.Fluid Mechanics*, 45, 209.
16. Milne-Thomson (1993) Theoretical Hydrodynamics. *Macmillan and Co., London*.
17. Parag Kumar (1993) Discrete vortex modelling of the wake of a flat plate. *M.Tech. Thesis, Indian Institute Of Technology, Kanpur*.
18. Porthouse D.T.C. and Lewis R.I. (1981) Simulation of viscous diffusion for extension of the Surface vorticity method to boundary layer and separated flows. *Journal of Mechanical Engineering science*, 23, 157-167.
19. Rosenhead L.(1931) The formation of vortices from a surface of discontinuity. *Proc. Roy. Soc.*, 134, 170-192.
20. Saffman, P.G. and Baker G.R. (1979) Vortex Interaction. *Ann. Rev. Fluid Mech.*, 11, 95-122.
21. Saffman, P.G.(1981) Dynamics of vorticity *J. Fluid Mech.*, 106, 49-58.
22. Sarpkaya T. (1975) An inviscid model of two-dimensional vortex shedding for transient and asymptotically steady separated flows over an inclined plate. *J.Fluid Mechanics*, 68, 109-128.

23. Sarpkaya T. (1989) Vortex induced oscillations *A.S.M.E. J. Appl. Mechanics*, 68, 109-128.
24. Shaff R. L. and Franks C.B. (1981) A discrete vortex analysis of flow about non-circular cylinders. *Proc. 3rd Int. Conf. on Numerical Ship Hydrodynamics, Paris*, 319-333.
25. Smith P.A. and Stansby, P.K. (1988) Impulsively started flow around a circular cylinder by the vortex method. *J. Fluid Mech.*, 198, 45-77.
26. Smith P.A. and Stansby, P.K. (1989a) An efficient surface algorithm for random-particle simulation of vorticity and heat transport. *J. Comp. Phys.*, 81, No. 2.
27. Widnall, S.E. (1975) The structure and dynamics of vortex filaments. *Ann. Rev. Fluid Mech.*, 7, 141-165.

